JVST A
Journal of Vacuum Science & Technology A

Investigating recent developments and applications of optical plasma spectroscopy: A review

Cite as: J. Vac. Sci. Technol. A **38**, 020806 (2020); https://doi.org/10.1116/1.5141844
Submitted: 08 December 2019 . Accepted: 05 February 2020 . Published Online: 24 February 2020

Angela R. Hanna, and Ellen R. Fisher

JVST A
Journal of Vacuum Science & Technology A

REVIEW

avs.scitation.org/journal/jva

Investigating recent developments and applications of optical plasma spectroscopy: A review

Cite as: J. Vac. Sci. Technol. A 38, 020806 (2020); doi: 10.1116/1.5141844
Submitted: 8 December 2019 · Accepted: 5 February 2020 ·
Published Online: 24 February 2020

Angela R. Hanna and Ellen R. Fisher[a)]

AFFILIATIONS

Department of Chemistry, Colorado State University, Fort Collins, Colorado 80523-1872

Note: This paper is part of the Special Topic Collection on 30 years of the Nellie Yeoh Whetten Award — Celebrating the Women of the AVS.

[a)]**Author to whom correspondence should be addressed:** Ellen.Fisher@ColoState.Edu

ABSTRACT

Optical spectroscopy is a powerful, nonintrusive diagnostic tool that can provide unparalleled insight into fundamental plasma properties. Specifically, these techniques are widely employed to qualitatively and quantitatively characterize interactions of species within a discharge. This work is comprised of two parts: (1) a brief review of recent literature on the application of optical emission spectroscopy from the past decade, ranging from the study of atomic rare gas to more complex environmentally and technologically relevant plasma systems and (2) the presentation of new data that illustrate the power of optical spectroscopy techniques beyond simple species identification. Specifically, time-resolved optical emission spectroscopy was utilized to provide kinetic information about excited state species formation, ultimately lending mechanistic insights into a range of plasma processes. In addition, by combining optical emission and broadband absorption spectroscopies, rotational and vibrational temperatures for both excited and ground state species were determined. These data provide a thermodynamic base for enhanced understanding of the fundamental chemistry in plasma systems. The two platforms explored here were plasma-assisted catalysis systems containing N_xO_y species and fluorocarbon plasmas utilizing a range of precursors to evoke either etching or deposition, depending on the plasma conditions.

I. INTRODUCTION

Optical emission spectroscopy (OES) is a widely used, relatively simple diagnostic tool for nonthermal plasmas at both low and atmospheric pressure. In the most straightforward configuration, OES only requires a means of collecting the emitted light, a dispersing element, and a detector.[1] Recent technological advances have, however, enhanced both the spatial and temporal resolution of spectrometers, leading to new applications and robust characterization of plasma processing. Indeed, the body of literature using OES to study plasmas has increased exponentially over the past decade, shown by the steadily increasing number of publications and citations in Figs. 1(a) and 1(b), respectively. This powerful technique can be employed to identify species, elucidate fundamental plasma properties, and monitor end-product formation in discharges. The most common use of OES by far, however, is species identification. Consequently, there are several noticeable gaps in the literature. For example, although plasmas are universally applied for surface modification strategies (i.e., etching, deposition, and modification), very few studies focus on the alteration of the gas phase of the plasma resulting from the presence of a substrate. Considering that the substrates being subjected to modification often have substantive electrical or catalytic properties, it is not difficult to imagine that the plasma properties could be significantly different with and without a substrate. The data in Fig. 1 also demonstrate the increased efforts of the plasma community in recent years to measure plasma temperatures and kinetics via optical spectroscopy. This approach can afford tremendous insights into the underlying mechanisms at work within the dynamic environment of a plasma. Furthermore, the types of data revealed from such studies are critical to the development of more accurate computer models of plasma systems, thereby increasing their predictive

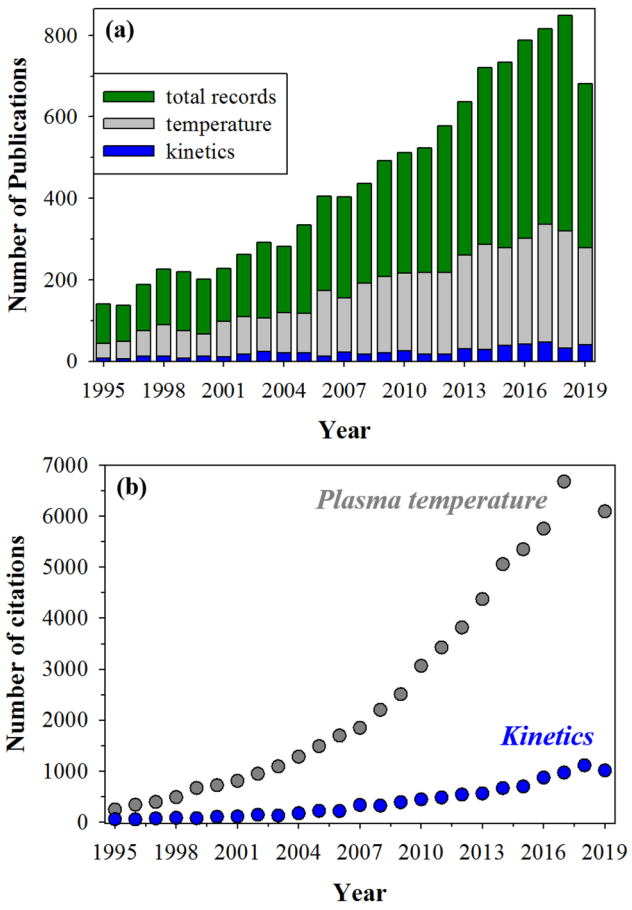

FIG. 1. History of research interest in plasmas investigated by optical emission spectroscopy, detailing (a) total publications and (b) sum of times cited per year for plasma temperature and kinetic studies since 1995 (Web of Science search on October 3, 2019).

power. Thus, the primary focus of this review will be on demonstrating how optical spectroscopy tools can be used, either alone or in combination, to provide valuable, formative data on the kinetics and thermodynamics of low-temperature plasmas. An additional aim of the current work is to highlight the contributions of women scientists to the plasma community within this Special Topic Collection: 30 Years of the Nellie Whetten Award, Celebrating the Women of the AVS. As such, a significant fraction of the cited works herein represents contributions from female researchers.

In the sections below, we provide (1) a brief literature review and background covering recent context for (2) the remainder of this work, which focuses on specific examples of how the Fisher group (both new and previously published work) has further explored the use of optical spectroscopy techniques to understand underlying plasma chemistry. We begin by using a relatively simple, highly studied system (e.g., Ar) to exemplify how OES can be used to characterize fundamental properties within noble gas plasmas. For example, nonthermal plasmas generally follow the empirical relationship wherein electron temperature (T_e) is significantly greater than the gas temperature (T_g) of the discharge.[2] Here, we discuss the application of OES to determine T_e as well as electron density (n_e), exploring how these parameters change temporally and as a function of operating conditions. Studying these fundamental plasma properties via OES in noble gas discharges represents a small fraction of the world of plasma diagnostics. Here, a review and discussion of new data are provided to highlight the utility of spectroscopy as a diagnostic tool for deconstructing the complexity within nonthermal plasmas. Specifically, molecules partition energy through vibrational and rotational degrees of freedom, which can be determined through the analysis of spectral transitions. By coupling energetic insights with temporally resolved kinetics, one can begin to unravel underlying mechanisms and chemistries in a variety of nonthermal plasma systems. Thus, we explore the utility of optical spectroscopies with a focus on comprehensive plasma diagnostics. Potential plasma-material synergisms in the context of plasma-assisted catalysis (PAC) systems containing N_xO_y species were also investigated, as well as several fluorocarbon (FC) discharges. These two platforms were chosen because they demonstrate a wide range of environmental and technological applications that can be achieved with nonthermal plasmas, as well as provide useful exemplifying data for each of the techniques covered herein.

II. LITERATURE REVIEW AND BACKGROUND

This section provides a concise literature review of recent articles describing the use of optical diagnostic techniques with a focus on pushing the capabilities of OES beyond simple species identification. The literature review provided is purposefully limited in scope by focusing on the past 10–15 years of published, peer-reviewed articles. It is not meant to be a fully comprehensive review but does include a necessary background for the data presented in subsequent sections, as well as coverage of pivotal studies that could be considered seminal to the development of new directions in optical spectroscopy techniques.

A. Spectroscopic studies of inert gas plasmas

Ionization, excitation, dissociation, recombination, and relaxation processes can occur as electrons transfer energy from the external field to the discharge gas.[2,3] As such, electrons play a crucial role in governing the overall plasma chemistry; understanding their behavior in these interrelated processes is thus critical to accurate modeling and simulation of plasma systems.[4] Although n_e and T_e are key parameters, they are often difficult to measure spectroscopically; rather, electrostatic Langmuir probes are often employed. Unfortunately, these probes physically perturb the plasma environment, which can be problematic, especially for depositing systems.[5] A direct, nonintrusive measurement of T_e is challenging, and many works have sought to establish a methodology based on the evaluation of OES emission lines in inert gas systems, with connection to detailed plasma modeling for verification.[6–11] Often explored within Ar plasmas, collisional-radiative (CR) technique uses a population density model determined by a system of rate equations, specifically considering collisional and radiative processes.[12] If one assumes a

local thermodynamic equilibrium (LTE) environment, population and depopulation processes are dominated by collisions; therefore, rates and distributions are governed by Boltzmann statistics and Saha equations.[2,13] Excitation transitions are primarily dominated by electron collisions; thus, if the discharge is operating in LTE, determination of an excitation temperature (T_{exc}) is an approximation for T_e, assuming the population of atomic excited states follows a Boltzmann distribution.[14] The validity of LTE assumptions has been investigated for a variety of discharge types.[6,15,16] Avoiding the inclusion of complex equilibrium models and intrusive probes, T_{exc} can be determined through the analysis of atomic emission lines via a Boltzmann plotting method. This technique, which naturally assumes a Boltzmann distribution, has been used for both low- and atmospheric-pressure plasmas, with comparison to traditional T_e determination methods (e.g., Langmuir probes).[3,17]

Plasma chemistry is largely governed by electron-mediated processes and thereby the electron energy distribution function (EEDF). Factors that influence the EEDF include discharge type, system pressure, and power.[18] Under equilibrium conditions, the EEDF follows a Maxwell–Boltzmann distribution, characterized by T_e and n_e; however, the EEDF of nonthermal discharges often deviates from a Maxwellian distribution due to temporal or spatial variation of electromagnetic fields, the presence of boundaries (e.g., reactor walls or substrates), and the absence of thermodynamic equilibrium (described in Sec. II C).[2,19] Often, despite these deviations, some portion of the EEDF is Maxwellian. As such, the practice of determining T_e assuming Maxwellian statistics is common, acknowledging the possibility of inherent errors in this simplification.[20] A Druyvesteyn EEDF is also commonly used to describe low-pressure plasmas, with the assumptions that the electric field strength is low enough to neglect inelastic collisions, T_e is significantly greater than T_i, and the collisional frequency is independent of electron energy.[2] Druyvesteyn distributions are characterized by a shift toward higher electron energies, compared to a Maxwell distribution.[2] Additionally, a bi-Maxwellian representation can be employed to model measured EEDFs, where a low energy or "bulk" electron population and the higher energy tail of the distribution are characterized by different temperatures.[21] The electrons in the high-energy tail of the distributions, though present in small concentrations, can have a significant impact on the overall reaction rates and plasma character.

Recently, several studies have implemented an emission line ratio technique for the determination of T_e and n_e, with comparison to trends obtained from electrostatic probes.[22–26] These measurements assume that excitation processes are dominated by direct electron impact and that subsequent depopulation from upper levels is either radiative or proceeds through collisional quenching. Both are reasonable assumptions for Ar plasmas operating at low pressure. Zhu and Pu detailed a variety of methods to determine T_e and n_e by line ratios for nonthermal Ar and N_2-containing plasmas, discussing the selection of appropriate line ratios and the limitations of the technique.[25] Several fundamental noble gas plasma studies explore the interdependence of T_e, T_{exc}, n_e, and plasma conditions.[7,10,27–31] The effect of plasma operating parameters on Ar ion and metastable number densities has also been with explored with the OES line ratio technique.[32,33] Although Ar is a widely studied plasma precursor and commonly used as an inert gas actinometer (discussed below), T_{exc} and line ratio studies were also included in this review to provide context for OES as a technique to characterize fundamental plasma parameters.

We note that obtaining absolute species concentrations from optical emission data is possible; however, this requires knowledge of electron impact rate constants, electron density, and energy distributions, as well as the absolute sensitivity of the spectrometer.[34] The determination of these properties can be quite difficult, especially as electron energies and distributions deviate from equilibrium within nonthermal discharges. Coburn and Chen were among the first to quantify the relationship between emission intensity and reactive particle density, thereby founding the technique of rare-gas actinometry in the plasma community.[35] To be as accurate as possible, this technique requires the actinometer and the species of interest to have similar cross sections for excitation, excitation thresholds, and excitation pathways.[36] Following the revolutionary work of Coburn and Chen, relative and absolute species densities within many plasma systems have been studied with OES. A brief overview of these studies that explored the relationship between gas-phase chemistry and a resulting plasma process is provided here.

To better understand the mechanisms of plasma-surface processing, regardless of the precursor or substrate, the role of gas-phase species in gas-surface interactions must be recognized. Donnelly and co-workers investigated the practice of adding traces of multiple rare gases (i.e., Ne, Ar, Kr, Xe) to a variety of etchant plasma systems to elucidate species density, T_e, and EEDFs via trace rare gases OES.[34,37,38] By examining T_e obtained from each individual gas, as well as various mixtures, the authors were able to differentiate and study different portions of the Maxwellian EEDF. Through the selection of emission lines primarily excited through electron impact of the ground state, electron temperatures were determined and differentiated for electrons within both the high-energy tail of the distribution and the lower energy, bulk electrons.[37] Fuller *et al.* measured absolute densities of Cl_2, Cl, Cl^+, and Ar^+ within inductively coupled (ICP) Cl_2-Ar plasmas, a system routinely utilized for the etching of semiconductor materials.[39] Absolute Cl atom densities have also been determined via actinometric OES in an ICP Cl_2 plasma, where a cylindrical substrate is rapidly rotated, creating a "spinning wall" effect.[40] Alshaltami and Daniels measured concentrations of oxygen and fluorine with OES and studied their impact on selective etching with SF_6-O_2 discharges.[41] Notably, in many industrial plasma processes, dry etch is performed without the addition of an inert gas as it can effect both etch rate and selectivity, hence inert gas actinometry is unviable. To address this, Kang *et al.* developed a "pseudo actinometry" technique for the normalization of species density in the absence of an inert gas.[42] A correction factor was experimentally determined by incrementally decreasing the number density of the inert gas within the discharge, eventually determining a convergence when the concentration of the inert gas was zero. The feasibility of the proposed technique was tested by the etching of Cr with a Cl_2/O_2 discharge, documenting strong correlation between Cl density distributions with Cr etch rate, determined via ellipsometry.[42] Thus, understanding species density within a plasma process can ultimately lead to process optimization, with and without an inert actinometer.

Another important consideration is how the relative concentrations of species are affected by the mere introduction of a substrate into the discharge. Cuddy and Fisher determined the density of CF and CF_2 species upon the addition of a substrate. Examining CF_4 and C_2F_6 plasma processing of Si and ZrO_2 wafers, they found that the presence of a substrate could dramatically affect the species density, and furthermore, this finding was substrate dependent.[43] Stuckert and co-workers monitored gas-phase species upon the addition of SnO_2 nanomaterial gas-sensors in H_2 radio frequency (rf) ICPs, a known reducing environment. The formation of both excited state OH* and Sn* in H_2 plasmas was observed when SnO_2 nanomaterials were present. As neither species is formed in H_2 or H_2/Ar plasmas without a substrate, they must be formed via plasma-surface interactions.[44] This study also introduced an additional level of complexity; micro- and nanostructured materials are more likely to strongly influence the plasma as compared to the effects of traditional two-dimensional materials (e.g., thin films and wafers). To better understand the mechanisms that govern plasma processes (i.e., modification through functionalization, etching, or deposition) of a specified surface, we must gain quantitative information concerning the kinetics and energetics of these complex systems.

B. Temporally resolved spectroscopy: Kinetic insights

The intricate dynamics occurring within plasma systems can be systematically and quantitatively probed with time-resolved (TR) OES. By employing TR-OES with an intensified charge coupled device (ICCD) camera, spatially and temporally resolved images can be obtained to study mode shifts and ionization events in discharges.[45] Gherardi *et al.* provided a detailed experimental and theoretical discussion regarding the increased use of ICCDs to study both physical and chemical properties of nonthermal plasmas, focusing on atmospheric plasma jets.[46] ICCDs can provide time resolution on the nanosecond scale, an important consideration of the study of streamers formed through nanosecond pulsed discharges.[47,48] Furthermore, TR-OES studies with ICCDs aid in the visualization of plasma dynamics,[49] where the temporal behavior of radiative species, T_g, T_e, and n_e, have been investigated within a variety of continuous wave (CW) and pulsed plasma systems.[50,51]

Pulsed plasmas are often used in the processing of materials to reduce substrate temperatures and prevent substrate damage, with the goal to increase uniformity of the overall plasma process.[52] Within pulsed systems, once the plasma pulses are off, an afterglow region can persist wherein energetic electrons recombine with ions to create neutral and excited state species.[53,54] Within Ar plasmas, that lower excited states are more populated during plasma ignition, whereas higher excited states are often more populated during the afterglow.[55,56] This hypothesis is further tested below, where TR-OES is employed to characterize the properties of pulsed rf Ar plasmas.

Additional studies have measured the evolution of species in the plasma afterglow during magnetron sputter deposition of Al_2O_3 and TiO_2 materials in direct current (DC) plasmas.[57,58] During these processes, Lopez *et al.* observed different Ar emission lines decayed with different rate constants, where the emission decay times (1–4 μs) were significantly longer than the radiative lifetimes of the Ar emitting levels.[57] The authors argue that these longer decay rates result from plasma dynamics and operating conditions, where the decay of fast electrons, Ar metastables, and Al and O atoms in the plasma afterglow (i.e., after plasma power is turned off) could be monitored via TR-OES. Within a pulsed DC magnetron Ar plasma, two decay times for different groups of Ar emission lines were found. The authors attribute the fast decay time (1 μs) to the decline of fast beam electrons in the plasma afterglow and the slower decay time (3.2 μs) to the decrease in Ar metastable density.[57] Hioki *et al.* argue that the decay of electron and ion densities, dissipation of electron energies, and metastable number density decrease will occur on different time scales.[59] Furthermore, the authors acknowledge the necessity to study low, moderate, and high energy electrons separately, as each may temporally decay differently.[59] Salmon *et al.* coupled TR-OES with a detailed kinetic model to determine the quenching rates of $N(^2P)$ atoms in the afterglow of an N_2 atmospheric pressure discharge.[60] Aforementioned, gaining quantitative experimental information on fundamental plasma properties can assist in plasma simulations. Specifically, the determination of quenching rates within pulsed N_2 plasma systems can have a substantial impact on the ability to build accurate models, with the potential for process improvement.

Significant technological applications can benefit from the use of TR-OES, such as the sterilization and cleaning of plasma chambers post film deposition. Bišćan and co-workers studied the removal of amorphous carbon film deposits on reactor walls by an oxygen plasma, where OES was employed for *in situ* monitoring of film deposition as well as O_2 plasma cleaning processes.[61] By measuring emissions from oxygen and hydrogen atoms, OH radicals, CH, and CO, alongside the documentation of plasma mode shifts during the cleaning of the plasma chamber, they were able to deduce when the system was free of impurities (i.e., hydrogen and carbon species) with improved accuracy over visual inspection.[61] This line of inquiry could easily be expanded to other film deposition systems, including the removal of fluorocarbon and chlorine contamination after plasma processing. Plasma cleaning studies are usually limited to searching for the disappearance or appearance (depending on experiment) of a given species in the gas phase, an inherently qualitative process. Of burgeoning interest, TR-OES can be quantitatively used to measure the initial production of plasma species, thus determining rate constants of formation through analysis of emission lines.[62] The ability to experimentally measure rate constants and reveal underlying plasma-surface mechanisms is presented below.

C. Energy partitioning between molecules and electronic states

Within nonthermal plasma systems, T_g is an important plasma parameter; it strongly influences the underlying chemistry that drives most plasma processes. T_g studied via OES has been shown to be highly dependent on plasma parameters, leading to an increased necessity to understand trends in energy partitioning.[63,64] The distribution of energy into rotational and vibrational degrees of freedom (expressed as temperatures T_R and T_V, respectively) is also an important consideration. The second positive

system of N_2 ($C^3\Pi_g \rightarrow B^3\Pi_u$) is commonly used to determine T_R and T_V in N_2 or N_2-containing plasma systems within low- and atmospheric-pressure discharges.[29,65–67] T_R values have long been employed as a measure of T_g,[68,69] with the assumption that rotational and collective translational temperatures (T_T) of the gas equilibrate within the plasma. Bruggeman *et al.* demonstrated that T_R only equilibrates with T_T when rotational energy transfer is relatively fast or nascent rotational distributions are thermalized.[63] Information gleaned from internal temperatures can elucidate the processes that dictate the overall character of the plasma, as the values are interrelated to species densities, T_e, formation reactions, and gas-phase and surface collisions of plasma species. Thus, elucidating energy partitioning trends [Fig. 1(b)] for a variety of excited state species, ranging from homonuclear diatomics (H_2, N_2, O_2) to species formed through the decomposition of a more complex precursor (e.g., CF from C_xF_y discharges) is a growing area of study.

OES provides useful kinetics and energetics data for emitting species; however, it is unable to directly evaluate ground state species within the plasma. Nevertheless, the rate balance equations for emitting species within the discharge can be employed to indirectly assess ground state neutrals via OES. Laser-induced fluorescence (LIF) is more commonly used to probe the ground state; however, this technique requires expensive laser equipment and is inherently limited to species that possess a fluorescing excited state.[1] Thus, broadband absorption spectroscopy (BAS), where a light source is interfaced with a high-resolution spectrometer, has recently found promise as an alternative technique for ground state species measurements, such as absolute species density and plasma energetics. Literature studies have used a range of light sources, including UV-enhanced Xe arc lamps,[70,71] deuterium-halogen lamps,[4,72,73] and light-emitting diodes (LEDs).[74–76] Compared to LIF, BAS is a viable strategy to determine absolute species density without intensive calibration procedures, discussed in depth in a recent review of atmospheric plasma characterization.[77] Liu and co-workers employed BAS to determine absolute density and rotational temperature of CF_2 radicals in capacitively coupled CF_4/Ar plasmas.[76] One of the difficulties with plasma absorbance measurements is the dual-reference nature of the system (i.e., both the light source and plasma are emitting), as well as poor signal-to-noise ratios. Wijaikhum *et al.* developed a two-beam ultraviolet-LED absorption technique, equipped with a probe and reference beam to improve the signal-to-noise ratio when measuring ozone densities.[75] In the present study, the utility of BAS to determine plasma temperatures in FC and N_2O discharges will be discussed. Moreover, our unique imaging radicals interacting with surfaces (IRIS) technique, which employs LIF spectroscopy, can provide insights into the behavior of radicals near substrates *during* plasma processing. Coupled with the kinetic and energetic information gained through gas-phase spectroscopy diagnostics, a more holistic understanding of gas-surface interactions is gained.

III. EXPERIMENT

The rf ICPs studied here were ignited in a glass tubular reactor, Fig. 2.[72] Relative base pressure (<1 mTorr) was maintained with a 400 l/min rotary vane mechanical pump. Gaseous precursors entered the reactor via a mass flow controller (MKS), where pressure (p) was monitored with a Baratron® capacitance monometer, ranging from 50 to 150 mTorr. Ar (Airgas, >99.999%), N_2 (Airgas, >99.99%), N_2O (Airgas, >99%), NO (American Gas Group, >95%), CF_4, C_2F_6, C_3F_8, C_3F_6 (all from Airgas, >95%), and HFPO (Sigma-Aldrich, 98%) were used in this work. Ar is often used as an inert gas actinometer within our plasma systems; therefore, high purity is utilized to avoid introducing additional gas species to the plasma system.

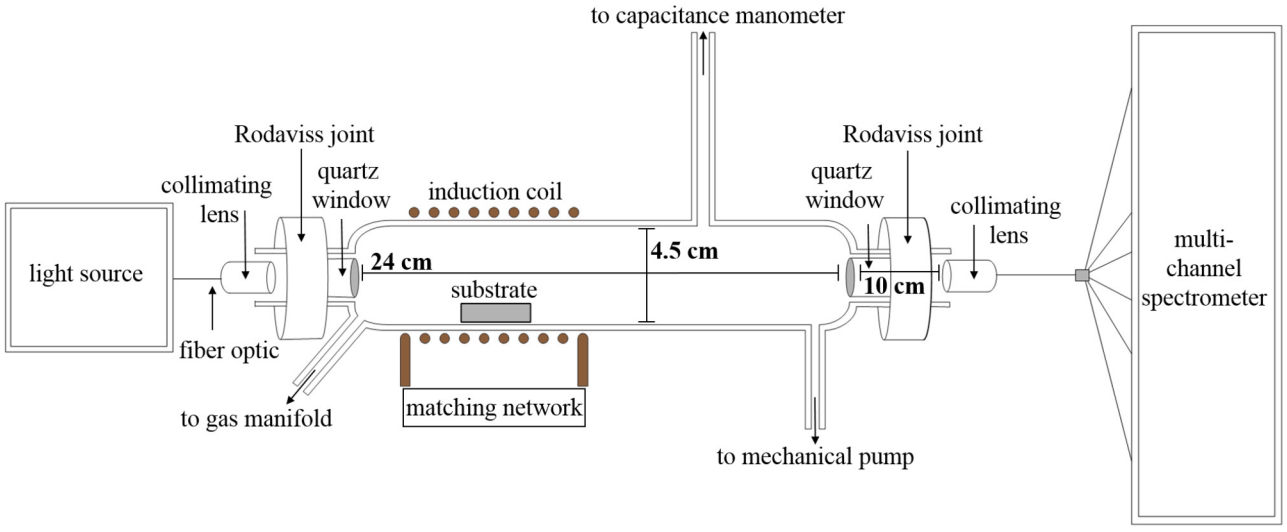

FIG. 2. Detailed schematic of OES/BAS apparatus used in spectroscopic investigations of low-temperature ICP discharges. Both collimating lenses are equidistant from quartz windows. Reproduced with permission from Blechle *et al.*, Plasma Process. Polym. **14**, 1700041 (2017). Copyright 2017, Wiley.

Applied rf power (P) was applied through a matching network using an rf power supply (model RFPP, Advanced Energy Industries, Inc.) at 13.56 MHz via an induction eight-turn-Ni-plated copper coil (Fig. 2).[72] CW P ranged from 5 to 200 W; pulsed power is reported in the form of a duty cycle (d.c.), defined here as the ratio of pulse on time to total cycle time, and equivalent power (P_{eq}), defined as product of the d.c. and the peak power. 20 and 10 ms pulse widths were used to study pulsed Ar and N_2 discharges, respectively.

Fused quartz windows at up- and downstream ends of the reactor were secured with RODAVISS® joints, enabling coaxial emission collection via collimating lens and fiber optic cables. The collimating lenses are equidistant from the fused quartz windows (10 cm). These reactors can be interchangeably interfaced to different diagnostic apparatus, with windows placed at different locations along the tubular reactor, allowing for OES collection at various spatial points along the reactor. An Avantes multichannel spectrometer (AvaSpec-2048L-USB2-RM) was utilized for all steady-state experiments herein; emission from 200 to 1000 nm was measured simultaneously with a spectral resolution of ~0.1 nm. A representative emission spectrum of an Ar plasma ($p = 100$ mTorr, $P = 20$ W) is provided in Fig. 3(a). A second spectrometer (AvaSpec-ULS4096CL-EVO) was employed in N_2 time-resolved studies for enhanced temporal resolution (i.e., microsecond time scale), with a spectral resolution of 0.5 nm. A Faraday cage was constructed around the plasma reactor and spectrometer(s) to minimize potential rf coupling between the discharge and electronics of the spectrometer.

The atomic emission intensity (I_{jk}) of the transition from level j to k depends on the Einstein coefficient of spontaneous emission (A_{jk}) and absolute population of the atomic level (n_j), shown in Eq. (1),[3]

$$I_{jk} = n_j A_{jk} h\nu, \tag{1}$$

where h is the Planck constant and ν is the frequency corresponding to the transition. Assuming the atomic level populations follow a Boltzmann distribution, I_{jk} is given by

$$I_{jk} = h\nu \left(\frac{A_{jk} g_j n}{U(T_{exc})}\right) \exp\left(\frac{-E_j}{k_B T_{exc}}\right), \tag{2}$$

where g_j is the statistical weight of level j, n is the number density of bound electrons (not to be confused with n_e pertaining to free electrons in the plasma), $U(T_{exc})$ is the partition function, k_B is the Boltzmann constant, and E_j is the energy of the upper level, j.[3] Equations (1) and (2) represent relationships for emitting species within ideal systems, not accounting for radiation trapping or electron distributions that deviate from a Boltzmann distribution. Excitation temperature (T_{exc}) was determined via the Boltzmann method, where $\ln(I_{ij}\lambda/g_j A_{jk})$ was plotted as a function of the upper level energy E_j, the slope of which is equal to $-1/k_B T_{exc}$. In Fig. 3(b), the experimental data for the higher Ar levels (quantum number $n \geq 5$) are linear with E_j, whereas lower lying levels (quantum number $n < 4$) deviate. This underpopulation of the lower energy state is a deviation from LTE, most likely resulting from plasma relaxation processes, rather than only through electron-impact excitation from the ground state followed by de-excitation.[78] Only the $n \geq 5$ Ar emission lines were utilized in the determination of T_{exc}; transitions (Paschen's notation) and relevant constants are listed in Table S1.[116] Although T_{exc} and T_e have been determined using analysis of Ar atomic lines, several studies have combined computational (CR models) and experimental (Langmuir probes) results to select emission line ratios with a high sensitivity to T_e and n_e, shown in Eqs. (3) and (4), respectively,[24]

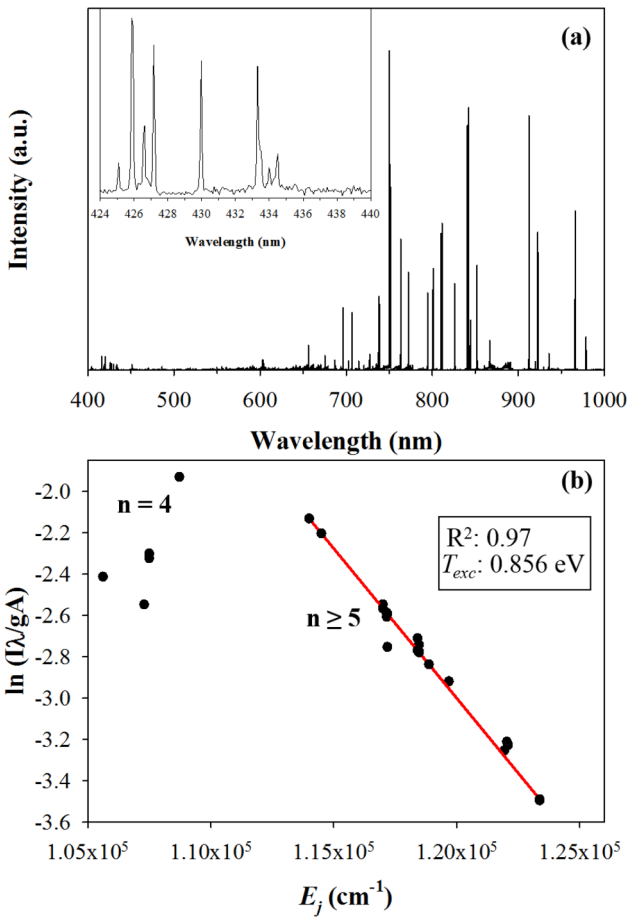

FIG. 3. (a) Representative emission spectrum and resulting (b) T_{exc} Boltzmann plot of Ar plasma (150 mTorr, 10 W).

$$T_e \text{ sensitive ratio} = \left(\frac{I(763.5\text{ nm})}{I\,(738.3\text{ nm})}\right), \tag{3}$$

$$n_e \text{ sensitive ratio} = \left(\frac{I(706.7\text{ nm})}{I\,(750.4\text{ nm})}\right). \tag{4}$$

Results from the T_e sensitive ratio [Eq. (3)] are compared to the T_{exc} values obtained via the Boltzmann plotting method for a range of system pressures (50–150 mTorr) and applied rf powers (5–50 W).

TR-OES data were collected to study the formation and decomposition mechanisms with atomic and molecular plasma systems. Data collection began before plasma ignition and lasted for ~5–10 s after ignition; integration times for TR-OES varied from 75 μs to 25 ms, depending on the experiment. Integration time determination is heavily influenced by the system of study, highlighted in Fig. 4. Emission arising from an N_2O plasma ($p = 100$ mTorr, $P = 150$ W) was collected at four integration times with one average, ranging from 50 up to 875 μs. Steady-state N_2O spectroscopy was previously collected at this experimental condition, revealing strong emission bands from N_2 second positive ($C^3\Pi_g \rightarrow B^3\Pi_u$) and NO ($A^2\Sigma^+u \rightarrow X^2\Pi$) transitions. As can be seen in the spectra in Fig. 4, at the fastest integration times, virtually no signal is observed for the NO and the N_2 signal is barely above the noise. As the integration time is increased slightly, emission bands from both molecules can clearly be seen in the spectra. This exemplifies the notion that the fastest integration time is not always optimal as emission from molecular species could get suppressed underneath poor signal-to-noise ratios. Therefore, selection of an integration time for a time-resolved study should be based on steady-state emission measurements to accurately include and assess species within a discharge.

The intensities of excited state species (e.g., CF and CF_2) were collected as a function of time, where the rise to maximum intensity was identified and fit with a first order exponential to determine the rate constant of formation (k_f).[62] A discussion of CF and CF_2 kinetics within C_xF_y plasmas as a function of power is provided in Sec. IV B.

Steady-state absorbance spectra were generated by collecting three irradiance-calibrated emission spectra: plasma (I_P), light source (I_S), as well as plasma and light source (I_{PS}). Absorbance spectra were produced using Eq. (5), following the example of

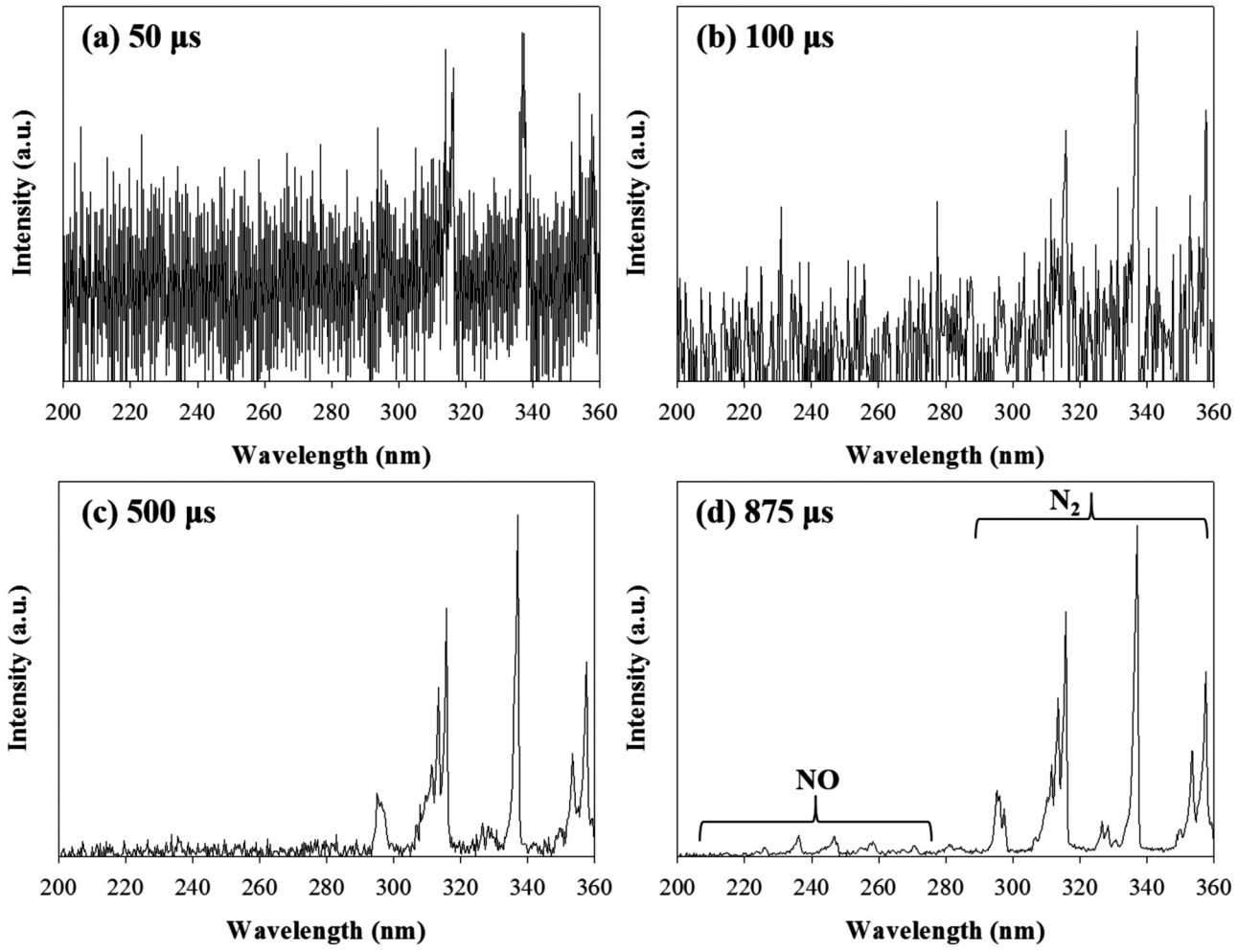

FIG. 4. N_2O plasma emission ($p = 100$ mTorr, $P = 150$ W) collected at four different integration times.

Bruggeman *et al.*[74]

$$A = -\left(\frac{I_{ps} - (I_p + I_s)}{I_s}\right). \quad (5)$$

$T_R(CF_2, N_2, \text{and NO})$ and $T_V(\text{CF and NO})$ values were determined from OES and BAS spectra using spectral fitting programs PGOPHER,[79] LIFBASE,[80] or SPECAIR.[81] A Boltzmann plotting procedure was also employed to determine emitting $T_V(N_2)$, described previously.[82] Determination of representative rotational and vibrational temperatures depends on the spectral resolution, quantum efficiency, and grating efficiency for each channel of the spectrometer. The wavelength-dependent quantum and grating efficiencies should be calibrated and corrected before the fit of measured spectra can be used for the determination of plasma temperatures, discussed previously.[72] All spectra collected herein are irradiance-calibrated across the wavelength range of 200–1000 nm; however, the grating efficiency reported by Avantes ranged from ~35% to ~65%, depending on the spectrometer channel. As may be expected, applying a correction for grating efficiency has no measurable effect on measured T_R values, as these are nominally determined by fitting the FWHM of the vibrational peaks. In contrast, the grating efficiency can impact determined T_V values. Notably, the differences in the resulting $T_V(\text{NO})$ values obtained with a grating efficiency correction compared to those obtained without a correction were, however, within the overall experimental error.[72] This can be rationalized by considering the methodology used to obtain $T_V(\text{NO})$ from emission spectra, which includes the entire vibrational band corresponding to the $A^2\Sigma_u^+ \rightarrow X^2\Pi$ transition in the simulated spectra. As a consequence, small differences in grating efficiency are likely accounted for within the fit of this relatively wide wavelength range (200–280 nm). For comparison, in the determination of $T_V(\text{CH})$ within CH_4 plasmas, we found the grating efficiency did have a significant impact on our results.[83] These data were, however, collected on a different four-channel Avantes AvaSpec-3648-USBS spectrometer.[83] In addition, the wavelength range for the CH ($A^2\Delta \rightarrow X^2\Pi$) molecule is significantly smaller (425–437 nm) and the $v' = 0$ and $v' = 1$ vibrational states significantly overlap in the CH vibrational band. By comparison, the NO emission band is characterized by distinctively separate vibrational peaks. Thus, small fluctuations in the grating efficiency within this smaller, more conflated wavelength range impacted the determined $T_V(\text{CH})$ values.[83] These examples clearly demonstrate that the potential influence of quantum and grating efficiencies, spectral resolution, and calibration technique should all be carefully considered when employing spectral techniques in plasma temperature determination.

Radical surface scatter coefficients (S) for NO and CF were measured using the LIF-based IRIS technique, described in detail previously.[84] Briefly, plasma afterglow from a reactor source expands into a differentially pumped region (base pressure ~10^{-6} Torr) to form an effusive molecular beam. Tunable laser light generated from an excimer-pumped (Lambda Physik LPX210i, XeCl 180 mJ/pulse, 25 Hz) dye laser intersects the plasma molecular beam at a 45° angle. LIF signals were collected for the molecular beam and beam interacting with a substrate. The difference between these images provides a measure of the signal arising from molecules scattered from a surface during plasma processing. The excitation wavelengths used were 223.838 and 226.199 nm for CF and NO, respectively. Cross sections along the laser propagation axis were taken from the center of most intense fluorescence for both the "beam only" and "scatter" images and fit with a geometrical model to derive S, as detailed previously.[85–87] The scatter coefficient is essentially a measure of the propensity for a particular type of species to scatter from, rather than react at or be consumed by, the surface. Note that S values may surpass unity, indicating the generation of radicals at the surface (e.g., via surface quenching of excited electronic state radicals, surface-mediated dissociation or recombination reactions). All scatter values herein have been previously reported.[4,72] Substrates included silicon wafers (p type ⟨100⟩), platinum foil (Alfa Aesar, 99.99%, 0.025 mm), platinum powder (Alfa Aesar, 99.99%), and zeolites (Sigma-Aldrich, 13x, 45/60 mesh molecular sieves) pressed into pellets.[82]

IV. RESULTS AND DISCUSSION

A. Fundamental Ar plasma studies

Noble gas precursors have been widely used as model systems to study the behavior of electrons within plasma discharges, especially Ar due to its relatively simple gas-phase chemistry, and availability of electron-impact cross section information.[20] Ar emission spectra are nominally dominated by the Ar I emissions, shown in Fig. 3(a) in the wavelength range of 650–1000 nm. As noted in the Secs. I and II, dilute amounts of Ar are often added to more complex systems as an inert gas actinometer to probe T_e and n_e, as well as determine relative and absolute species densities, as a function of plasma operating conditions. Within nonthermal ICPs, it is generally recognized that the primary effect of increasing rf P is to increase plasma density at a fixed pressure, where T_e is hypothesized to be relatively independent from plasma power.[2,13] Several works, however, have experimentally observed T_e fluctuations over a range of powers in rf ICP discharges. Lee *et al.* measured changes in T_e as a function of power in Ar rf ICPs, ignited at 13.56 MHz via an antenna coil, with both Langmuir probe and laser Rayleigh scattering measurements.[88] This study was performed at $p = 50$ mTorr, $P = 100$–900 W, where the authors claim that T_e decreases as the power increases from 100 to 500 W and then increases with $P = 500$–900 W. The measured T_e values, however, are within experimental error of each other at several P conditions, with all of the values falling in a narrow range of ~1.81 to ~2.10 eV.[88] As such, it is challenging to understand whether the claims of a local minimum in T_e with power are valid or if it might be translatable to other systems. Consequently, we sought to perform a similar characterization of our rf Ar plasmas by using OES to examine our systems as a function of small changes in power ($\Delta P = 5$ W) at three different plasma pressures.

Figure 5(a) shows calculated T_{exc} (eV) values as a function of plasma operating conditions, revealing several interesting trends regarding pressure, power, and discharge mode. At $P \leq 15$ W, there is a clear pressure dependence: increasing system pressure from 50 to 150 mTorr can increase the frequency of collisions; hence, a quenching of T_{exc} is observed. Within the 150 mTorr system, as P increases from 15 to 20 W, the discharge visually changes,

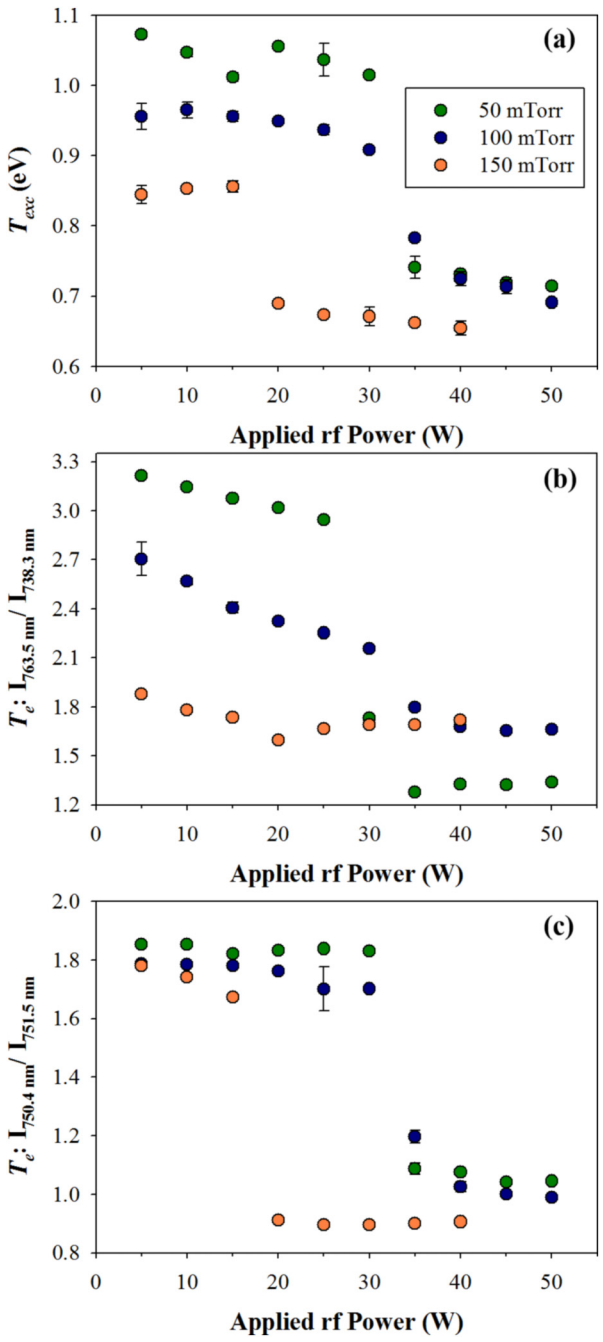

FIG. 5. (a) Calculated T_{exc} values, T_e sensitive line ratios (b) ($I_{763.5\ nm}/I_{738.3\ nm}$) and (c) ($I_{750.4\ nm}/I_{751.5\ nm}$) determined in Ar plasmas, plotted as a function of p and P.

indicating a shift from operating in capacitive (E) to inductive (H) mode, and a corresponding sharp decrease in T_{exc} was also observed. Generally speaking, a discharge operating in the E mode is sustained by the electrostatic field and is characterized by a low plasma density; the H mode is sustained by applying more power or current, subsequently creating a system characterized by higher plasma density.[89] Above $p = 150$ mTorr and $P = 40$ W, emission from the plasma saturated the detector and no additional spectral data could be reliably collected. At lower pressures (50 and 100 mTorr), the visual mode change occurred at higher power, between 30 and 35 W. When the plasma operates in the E mode or H mode, regardless of pressure, small fluctuations in T_{exc} may be observed as a function of rf power; nevertheless, the majority of these data are within experimental error. Notably, the largest changes in T_{exc} occur when the plasma shifts between modes.

A considerable number of studies have sought to use the intensity ratio of two OES lines to determine T_e and n_e trends as a function of plasma operating conditions. The sensitivity and potential accuracy of these measurements will, however, strongly depend on the choice of line ratios.[24] The selection of emission line ratios is largely dependent on the major collisional-radiative processes within the discharge and are theoretically supported by a population model (e.g., Corona and collisional-radiative models).[25] Therefore, system pressure and ionization rate, as well as the EEDF, plasma dimension, and gas temperature can influence the population and depopulation processes and thereby the selection of line ratios. Discussed above, the plasma can shift between capacitive and indicative modes based on operating conditions; therefore, the plasma mode may also play a role in the determination of T_e via OES line ratios. Boffard *et al.* studied rf ICP plasmas at 13.56 MHz at $p = 10$–50 mTorr and $P = 600$ W, using the ratio of line intensities at 420.1 and 419.8 nm to measure the effective T_e in Ar-containing systems, finding temperatures obtained with this line pairing in ICPs are consistent with those determined via a Langmuir probe.[23] Siepa and co-workers studied 13.56 MHz rf driven, capacitively coupled plasma (CCP) discharges, at $p = 20$ Pa (~150 mTorr) and 200 Pa (1.5 Torr) at $P = 50$–350 W, using the ratio of line intensities at 763.5 and 738.4 nm to examine T_e.[24] We also employed this line ratio to examine our Ar rf ICPs at $p = 50$–150 mTorr and $P = 5$–50 W [Fig. 5(b)]. Upon comparison to calculated T_{exc} values, a similar pressure trend emerges when the plasma is operating at low P (i.e., in the E mode); however, there appears to be a stronger P dependence with the line ratio method than with the T_{exc} values, determined via the Boltzmann plot [Fig. 5(a)]. Furthermore, a sharp drop in T_e (line ratio method) corresponding to an E to H mode transition is not observed for the 150 mTorr system, although visually the plasma has switched operating modes. Furthermore, at $P = 40$ W, the T_e line ratios suggest that a lower T_e is obtained with a lower system pressure, which conflicts with expected ionization balance within a discharge and the T_{exc} trends shown in Fig. 5(a). Similarly, however, Chai and Kwon observed a drastic increase in the relative intensities of 811.5 and 763.5 nm emission lines with increasing Ar pressure within a CCP at 13.56 MHz.[7] The authors attribute this intensity increase to radiation trapping, an argument supported by the results of their CR modeling.[7] The potential susceptibility of the Ar $2p_6$ (763.5 nm) line to radiation trapping at increased pressures could further explain the discrepancies in Fig. 5(b). Ar $2p_1$ (750.4 nm) and $2p_5$ (751.5 nm) emissions are primarily produced by ground state excitation, whereas other Ar (2p) levels are produced by both ground- and metastable-state excitations.[20] The $2p_1$ and $2p_5$ lines have shown sensitivity to T_e at

$p = 120$ Pa (900 mTorr);[25] Donnelly employed these emission levels to determine high T_e (characterizing electrons in high-energy tail) in combination with additional Kr and Xe lines.[37] Figure 5(c) depicts the $2p_1/2p_5$ ratio as a function of system pressure and power. Here, pressure effects are diminished at lower powers (i.e., E mode) for this line ratio compared to T_{exc} [Fig. 5(a)] and results from $2p_6/2p_3$ ratio [Fig. 5(b)]. Notably, the trends in Figs. 5(a) and 5(c) are better aligned at higher powers (i.e., H mode). These data suggest that discharge mode should be an additional consideration when applying the line ratio method to assess T_e trends within a discharge.

Additionally, the discrepancies presented in Fig. 5 highlight the necessity for careful selection of line ratios, as well as comparison to other computational and experimental techniques, such as population models and Langmuir probes. A previous Fisher group study characterized Ar ICPs at $p = 30$–50 mTorr and $P = 25$–150 W with Langmuir probe and mass spectrometry measurements.[90] At 25 and 50 W, little to no pressure dependence is documented; however, at the highest P (150 W), T_e decreases from ~3.75 to ~3.0 eV as p increases from 30 to 50 mTorr. Although different operating conditions were employed, this same trend is reflected in Figs. 5(a) and 5(c); however, the values of T_{exc} are considerably lower compared to T_e measured with a Langmuir probe. Further comparison reveals that although the type of plasma was consistent between these studies (rf ICP), the plasma dimensions and discharge volume differed, which may contribute to the difference in T_{exc} and T_e. As described above, a bi-Maxwellian distribution can be used to describe plasmas that contain both a high T_e (electrons in the tail of the distribution) and a low T_e corresponding to bulk electrons. By assuming a Maxwell–Boltzmann distribution to determine T_{exc} in our current studies, it is likely that we are primarily characterizing the bulk electrons, providing a lower limit for T_e compared to the T_e values obtained directly with the Langmuir probe of a similar system.

Electron density (n_e) is an additional plasma parameter that can be characterized through the OES line ratio method (Fig. 6). At 50 and 100 mTorr, there is little power dependence when the plasma operates in the E mode (5–30 W); at $P = 35$ W, however, a sharp increase by a factor of ~3 is documented. Revealed via a global model analysis, an increase in system pressure leads to a decrease in electron temperature and concomitant increase in plasma density, presented through n_e determination.[91] The 100 mTorr system continues to increase until 40 W, then little power dependence is observed in the H mode operation at 50 or 100 mTorr. Although a similar trend is observed for the 150 mTorr system, the mode transition occurs at lower P (15 → 20 W). An additional n_e sensitive line ratio ($I_{696.5\text{ nm}}/I_{750.4\text{ nm}}$) was proposed by Crintea *et al.*;[92] within our rf ICP system, this ratio yielded similar results to those shown in Fig. 6 for the ($I_{706.7\text{ nm}}/I_{750.4\text{ nm}}$) ratio.

As noted in the Sec. II, these plasma properties are widely studied and can be system-dependent, and therefore important to characterize for each discharge type and reactor setup. Therefore, we sought to probe how incremental increases in power could influence fundamental plasma properties. In a previous Ar ICP study, a positive correlation with n_e and rf power was measured with a Langmuir probe; however, this study was performed over a large power range ($\Delta P = 125$ W).[90] Moreover, the density of ions increased from $\sim 1 \times 10^{10}$ to $\sim 5 \times 10^{10}$ cm^{-3} as power increased

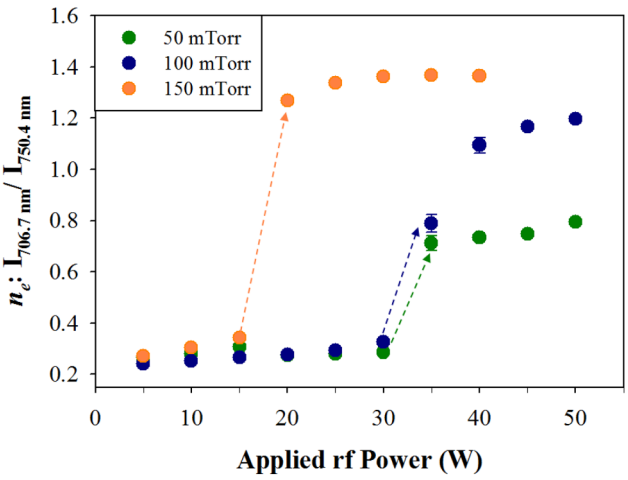

FIG. 6. n_e sensitive line ratio ($I_{706.7\text{ nm}}/I_{750.4\text{ nm}}$) determined in Ar plasmas as a function of p and P. Dashed lines represent a change from plasma operating from E mode to H mode.

from 25 to 150 W. As power increases, that energy can be distributed to the formation of more Ar ions or higher energy metastable states.[90] Wang *et al.* compared effective electron temperature (T_{eff}) values measured via probe and OES analysis of a Ar ICP operating at 600 W, $p = 1$–25 mTorr, documenting that as system pressure increases, T_{eff} decreases with a parallel increase in n_e. The data shown in Figs. 5 and 6 reflect these relationships between plasma properties and pressure. Recently, the study of fundamental plasma properties (T_e, n_e, and T_g) was expanded by Durocher-Jean *et al.* with small admixtures of N_2, O_2, and H_2 into microwave Ar plasmas at atmospheric pressure.[93] Each of these admixtures are common plasma precursors with their own physical and chemical properties; therefore, the authors sought to understand how the addition of these gases contribute to the overall plasma character. At the highest amount of admixture in the Ar plasma (1%), T_g generally increased with a concomitant decrease in n_e. As systems become more multifaceted, it is imperative to understand how fundamental properties evolve with increased complexity.

To further explore the relationship between electron dynamics and plasma conditions, TR-OES was employed to probe pulsed Ar plasmas, monitoring the 750.4 nm ($2p_1$) line and T_e line ratio ($2p_1/2p_5$) as a function of time, shown in Figs. 7(a) and 7(b), respectively. Figure 7(a) contains TR-OES data for a pulsed Ar plasma ($p = 100$ mTorr), collected with a 50% d.c. at three different P_{eq}. Although there are clear intensity differences for the powers studied, the shape of the pulse is relatively independent of P_{eq} and the plasma operating mode. Figure 7(b) depicts temporally resolved T_e line ratios for an Ar plasma ($p = 100$ mTorr) at three operating conditions, with $P_{eq} = 5$, 20, and 50 W. At $P_{eq} = 5$ W, T_e ratios increase sharply to ~2.0 at the start of the second and fourth pulses, with a subsequent decay to ~1.6. Boffard and co-workers monitored the 420.1–419.8 nm emission lines of Ar to elucidate temporally resolved T_e, documenting enhanced T_e at the start of the pulse (time resolution 25 μs),

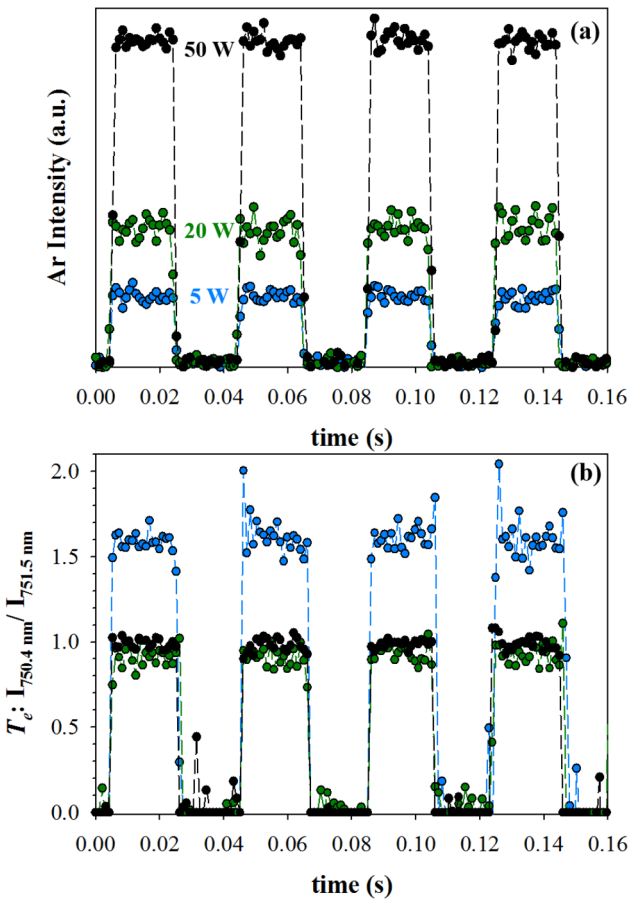

FIG. 7. TR-OES of pulsed Ar plasma (p = 100 mTorr, 50% d.c.) at (a) P_{eq} = 5 W, 20 W, and 50 W and (b) corresponding T_e line ratios ($I_{750.4\ nm}/I_{751.5\ nm}$).

followed by a decrease to a steady value within the cycle.[94] The tendency of T_e to overshoot steady-state values at the beginning of the active glow (plasma-on) and subsequent decrease to a steady-state value during the pulse cycle has been observed previously in both theoretical and experimental studies.[52,95,96] These initial "hot electrons" were not detected at every cycle or P_{eq} in our pulsing experiment; however, the TR-OES data shown in Fig. 7 were collected with a 1.05 ms integration time, whereas the time resolution in the Boffard study was 25 μs.[94] Therefore, the sharp increase or overshoot of T_e at the beginning of the active glow is likely occurring consistently, albeit sometimes on a time scale experimentally unavailable with our current apparatus. In the afterglow (plasma off), Boffard *et al.* noted significant electron cooling,[94] where T_e decreases rapidly due to inelastic collisions and fast electron escape to the wall, effectively approaching gas temperature due to diffusional cooling.[95] Specifically, Godyak measured T_e = 0.05 eV in the afterglow in an Ar ICP (4 MHZ) discharge at 3 mTorr.[95] Pulsing the discharge not only changes the applied power but also modifies plasma parameters such as plasma sheath formation, potentials across the sheath, which in turn affects ion and electron energies.[97]

Depicted in Fig. 5(c), within a CW Ar plasma (100 mTorr, 20 W), the plasma is operating in the E mode with a T_e line ratio value of 1.76. As power is increased to 40 W, the plasma shifts modes and the T_e line ratio value decreased to 1.026. Studying the pulsed Ar system (P_{eq} = 20 W, peak power = 40 W), the plasma was visually operating in the H mode. In Fig. 7(b), the line ratio technique yielded a T_e value of ~1 for both P_{eq} = 20 and 50 W, quantitatively indicative of H mode operation. Lieberman and Ashida employed global models to study pulsed and continuous wave Ar discharges to describe the behavior of plasma density and electron temperature. Assuming a Maxwellian EEDF, they found that the time-averaged plasma density can be considerably higher (up to four times greater) than that for CW discharges for the same time-averaged power.[98] Additionally, at P_{eq} = 5 W, a T_e value of ~1.6 was obtained, where the CW discharge resulted in T_e = 1.78. This discrepancy is unsurprising, as Logue and Kushner report that steady-state T_e values in the active glow may differ from T_e within a CW discharge, even if ignited at the same P_{eq}.[99] By employing OES as a diagnostic tool, one can probe fundamental plasma properties as a function of time, effectively assessing the differences between CW and pulsed regimes of a discharge.

OES can also be used to characterize streamers generated by nanosecond pulsed discharges. Goekce *et al.* measured plasma dynamics with a spectrometer coupled with an ICCD camera to achieve a time resolution of 2 ns, determining the average reduced electric field associated with surface streamers using transitions arising from atmospheric-pressure air plasmas: Ar transitions ($4p_x$–$4s_y$), as well as the first negative system of N_2^+ ($B^2\Sigma_u^+$–$X^2\Sigma_g^+$), and the first positive ($B^3\Pi_g$–$A^3\Sigma_u^+$) and second positive systems ($C^3\Pi_u$–$B^3\Pi_g$) of N_2.[47] For pulsed plasma systems, a faster time resolution than the one reported here is clearly critical if monitoring nanosecond pulse widths in comparison to the 10 ms pulse widths reported here. Clearly, however, the desired time resolution for a given experimental must be chosen carefully as it will depend heavily on the nature of the discharge, such as CW or pulsed, as well as the type of species to be monitored, whether molecular or atomic precursors or products of precursor decomposition (Fig. S1).[116] In Sec. IV B, we expand the examination of time-resolved studies of pulsed plasmas to more complex and technologically relevant systems.

B. Application-focused time-resolved spectroscopy

Large bandgap nitride materials have become increasingly important in catalytic and semiconductor processes. Nitrogen doping via plasma modification can enhance chemical and electrical properties of a wide variety of materials, ranging from metal oxides to carbon nanostructures.[100,101] In a recent study, we documented the implantation of N into TiO_2 and zeolite substrates with a CW N_2 rf plasma.[82] To extend this study here, we used TR-OES to characterize pulsed N_2 plasmas (P_{eq} = 175 W, 50% d.c.), with and without a porous zeolite substrate in the coil region. For the N_2 system without a substrate, Fig. 8(a) shows that the intensity of N_2 emission (337.0 nm) slightly decreased through the duration of the 10 ms pulse widths, and little to no signal arising from NO (235.9 nm) was observed. Similar to the Ar system data in Fig. 7, we observe "hot electrons" at the initiation of the pulse. Upon addition of a zeolite, a signal from NO appears [Fig. 8(b)] suggesting its

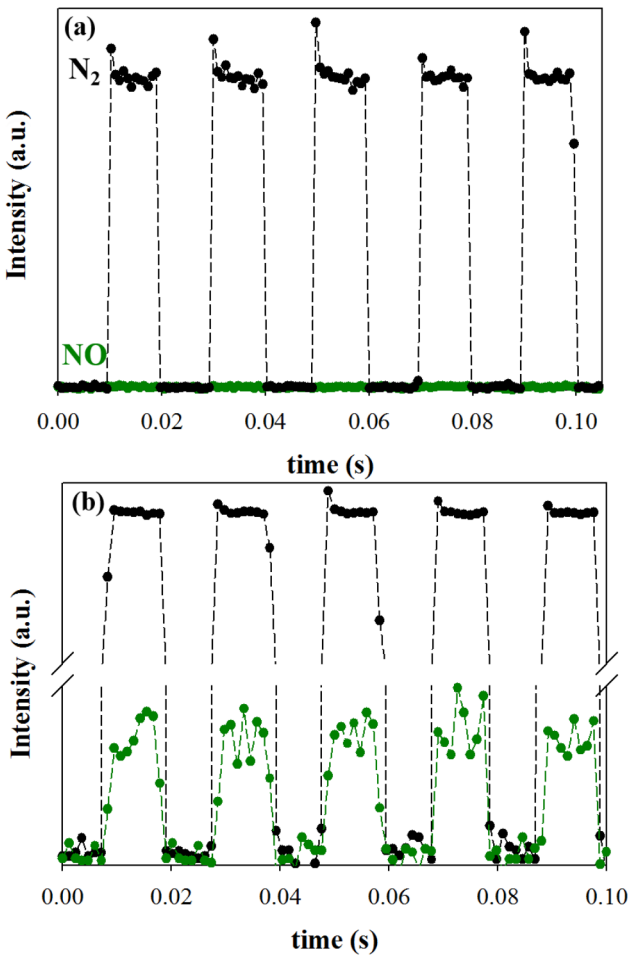

FIG. 8. Time-resolved intensity of N_2 and NO with (a) no substrate and (b) a zeolite pellet in the coil region of an N_2 pulsed plasma ($p = 100$ mTorr, $P_{eq} = 175$ W, 50% d.c.).

formation in the system arises from the removal of surface oxygen. With the zeolite substrate, the signal from "hot electrons" is less discernable in the emission signal from N_2. In comparison to our data, Mackus *et al.* used TR-OES to study pulsed plasmas used in atomic layer deposition (ALD), providing a mechanism for monitoring thin-film growth in real time.[102] By monitoring emission intensities during plasma processing, the authors determined failures in plasma ignition during ALD cycles and could pinpoint the time at which gas flow failed. The ability to use TR-OES as an *in situ*, nonintrusive method to monitor and detect a range of advanced material manufacturing techniques could substantially impact the adoption of industrial ALD processing.[102]

As a second example of the use of OES to establish optimal processing conditions, we turn to FC systems that are widely utilized to etch or deposit materials in the semiconductor industry. Specifically, gas-phase species (e.g., CF and CF_2) are hypothesized to contribute to FC film deposition. Using TR-OES, the production of CF and CF_2 from FC precursors was determined, ultimately providing kinetic information on important film-propagating species.[62] Figure 9 shows rate constants for the formation of CF and CF_2 as a function of P, for a variety of C_xF_y precursors.[62] Notably, these calculated rate constants reflect the production of excited state CF and CF_2 species in the gas phase but do not specify mechanisms of formation. The formation kinetics of CF and CF_2 within CF_4 plasmas, an etchant system, strongly deviate from those observed in the other C_xF_y systems, which are more commonly used for film deposition. Specifically, k_f(CF) values for CF_4 plasmas increase linearly (linear regression metrics: slope = 0.038 and $R^2 = 0.999$, not shown) as a function of P. In contrast, $k_f(CF_2)$ values obtained in the CF_4 system are an order of magnitude lower than those measured in all other C_xF_y systems, with no appreciable P dependence. These data suggest that the initial decomposition of the CF_4 precursor ($t \approx 0.5$ s) favors

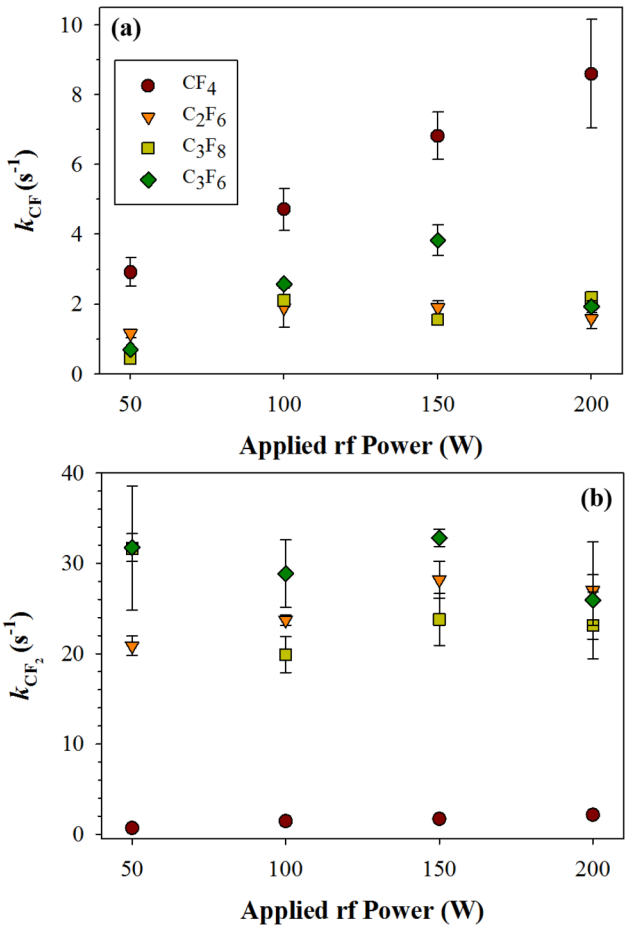

FIG. 9. Rate constants for formation of (a) CF and (b) CF_2 in C_xF_y plasmas obtained from time-resolved analyses of 202.4 and 251.9 nm OES lines are plotted as functions of P. Reproduced with permission from Cuddy and Fisher, Appl. Mater. Interfaces **4**, 1733 (2012). Copyright 2012, American Chemical Society.

the production of CF over CF_2 species as P increases. For plasmas with y/x ratios <4.0, $k_f(CF_2)$ values are effectively constant, regardless of precursor or P and are an order of magnitude higher than $k_f(CF)$ values obtained for the same precursors. Thus, the etching character of CF_4 plasmas is hypothesized to arise from the comparative lack of film-forming or film-propagating units (e.g., CF_2) in the gas phase.[62] Although C_xF_y systems with lower y/x ratios have been documented to deposit FC films more readily than high ratio feeds, CF_4 film deposition pathways are still largely unidentified. Plasma gas-phase diagnostics can elucidate species and processes responsible for FC etching and depositing processes. The two FC systems described here clearly demonstrate that using *in situ* TR-OES to quantitatively assess gas-phase phenomena during the processing of materials can be applied to a wide range of systems, regardless of end application.

C. Energy partitioning within N_xO_y plasmas

As noted in Secs. I and II, optical spectroscopy can be used to determine a range of characteristic temperatures for plasma species. In particular, determining internal temperatures for plasma molecules allows us to understand more fully how energy is partitioned within a particular system and how that partitioning may change as a function of various system parameters. Figure 10 depicts representative emission [Fig. 10(a)] and absorbance [Fig. 10(b)] spectra for an N_2O plasma system ($p = 100$ mTorr, $P = 150$ W), along with simulated fits of the NO ($X^2\Pi$–$A^2\Sigma^+$) and N_2 ($B^3\Pi_g$–$C^3\Pi_u$) bands.[73] In this system, T_R values for both NO and N_2 are significantly lower than T_V values, demonstrating the enhanced thermalization of rotational states in our plasmas. Determination of excited state $T_R(N_2)$ via OES is often used as a proxy for obtaining the overall T_g within a nonequilibrium plasma. The validity of such practice was discussed extensively by Bruggeman and co-workers and is beyond the scope of the current work.[63] As a general rule, however, Bruggeman and co-workers found that such practice requires caution as there are many examples where T_g is not well represented by internal molecular temperatures. As shown in Fig. 10(c),[73] a clear, linear relationship exists between P and T_V for both emitting and absorbing species in the N_2O system. As power increases, more energy is being supplied to the discharge; our data suggest this energy is partitioned into the gas-phase species, resulting in higher vibrational levels within the electronic transitions being populated. Here, the N_2 ($C^3\Pi_u$) and NO ($A^2\Sigma^+$) species displayed the highest and lowest vibrational temperatures, respectively. Considering the well-known potential energy surfaces of these molecules, the first excitation of NO from the ground electronic ($X^2\Pi$) to first excited ($A^2\Sigma^+$) state requires ~5.4 eV,[103] whereas the energy separation between the N_2 ($B^3\Pi_g$) and ($C^3\Pi_u$) states is only ~3.7 eV.[103] Therefore, lower vibrational levels within the NO ($A^2\Sigma^+$) state are populated because of its larger energy gap, ultimately resulting in a lower T_V.

Understanding how these factors change as a function of operating conditions can help tailor experimental design for a wide range of applications. Indeed, these data clearly aid in the description of steady-state energetics within N_2O discharges; however, it is also important to consider how energetics can evolve within the system over time and with the addition of an active (e.g., catalytic)

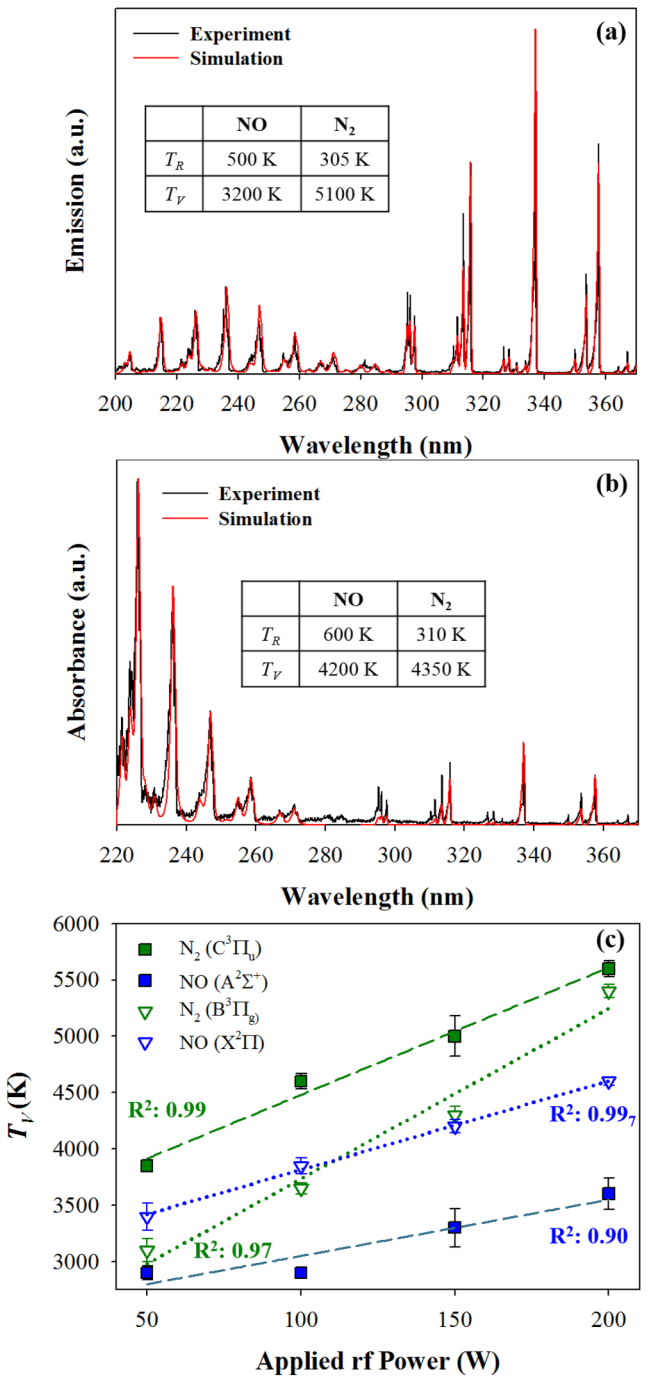

FIG. 10. Representative (a) emission spectrum and (b) absorbance spectrum for an N_2O plasma ($p = 100$ mTorr, $P = 150$ W). Inset tables report the T_R and T_V values obtained from the simulated fit of each molecule. (c) T_V values for N_2 and NO are plotted as a function of P ($p = 100$ mTorr). Error bars represent ±1 standard deviation from the mean ($n \geq 3$). Reproduced with permission from Hanna *et al.*, J. Phys. Chem. A **121**, 7627 (2017). Copyright 2017, American Chemical Society.

substrate. TR-OES data (25 ms integration time) were collected for an N_2O discharge operating at 100 mTorr for ~10 s after ignition. Figure 11(a) shows the temporal evolution of $T_V(N_2)$, determined via a Boltzmann plotting procedure using a Python code to analyze large data sets (i.e., >3000 scans). The horizontal lines correspond to the steady-state vibrational temperature determined at each power. As previously described and shown in Fig. 11(a), $T_V(N_2)$ increases with increasing P, where T_V values determined at $t = 0$ are also power dependent (75 W: ~2000 K; 125 W: ~2500 K; 175 W: ~3000 K). Interestingly, the rise to a steady-state temperature follows a first order exponential, and the slope of that rise varies with rf P. Note also that the T_V values measured under steady-state conditions are reflected in these time-resolved data and are reached within ~1 s, with the $P = 175$ W system taking the longest to achieve steady state. These data exemplify the need to study the temporal evolution of energetics within these systems; the nuances of excited state species formation and energy distributions would not have been documented with only steady-state optical experiments.

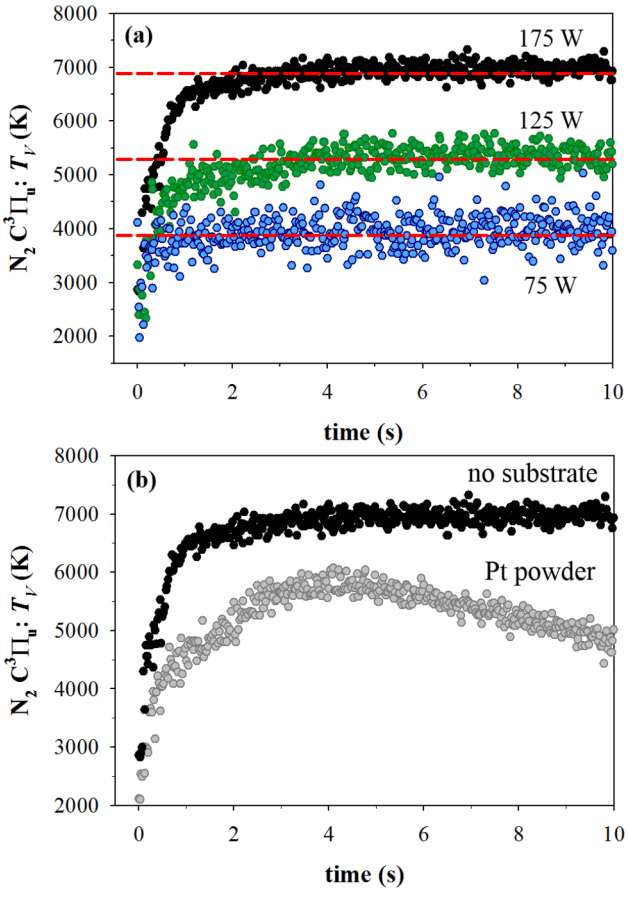

FIG. 11. T_V (N_2) within an N_2O plasma ($p = 100$ mTorr), determined as a function of time at (a) $P = 75$–175 W and (b) $P = 175$ W with no substrate and Pt powder present. Horizontal lines correspond to T_V (N_2) determined from steady-state OES.

A current area of interest to the plasma community, PAC, seeks to understand the synergistic coupling of a plasma with a catalyst for improved pollution abatement.[104,105] In our lab, a goal of this work is to understand how the catalytic material can impact the resulting kinetics and energetics of gas-phase species.[82] Figure 11(b) contains TR-OES data for $T_V(N_2)$ formed in an N_2O plasma ($p = 100$ mTorr, $P = 175$ W) with and without a Pt nanopowder catalyst. These data show that the temporal evolution of $T_V(N_2)$ changes dramatically by including the catalyst in the plasma. When the catalyst is present, $T_V(N_2)$ is always lower by ~1000–2000 K during the experiment. Moreover, rather than achieving a steady-state $T_V(N_2)$ value after the initial rise in the signal, the Pt power data appear to rise much more slowly with time up to ~4 s, decreasing steadily at longer times. Although it is unclear from these data whether a steady-state $T_V(N_2)$ value is achieved at longer times, the difference in temporal behavior is intriguing. One possible explanation for this comes from the selective energy transfer (SET) model of kinetics.[106–108] SET suggests that within a given catalytic system, excitation and decomposition of a specific molecule by a specific catalyst occurs via a vibrational resonance effect. In the traditional application of the SET model, it is the catalyst that supplies the necessary energy to achieve higher vibrational levels within the molecule to achieve decomposition.[108] Given the high vibrational temperatures of the excited plasma species in our PAC systems, it is plausible that the energy transfer occurs in the opposite direction from the molecule to the catalyst through the same vibrational resonance. Notably, in many of the SET systems reported in the literature, little chemisorption of the intact molecule onto the catalyst surface is observed, depending on the catalyst.[107] This does not, however, take into account any competing or contributing reactions occurring simultaneously. Nevertheless, the use of TR-OES greatly expands the utility of the OES technique by providing a mechanism to glean kinetic information about the plasma and to perform temporal investigations of plasma-substrate interactions.

D. Probing plasma-substrate interactions by coupling diagnostic techniques

Another feature of our OES-related studies entails *in situ* measurements of steady-state plasma-substrate interactions. Specifically, our unique LIF-based IRIS technique was coupled with OES measurements to investigate potential synergisms between a molecule's propensity to scatter and excited state vibrational energy. As documented in previous studies and shown here [Fig. 11(b)], the presence of a substrate can have a substantial impact on T_V.[82] Thus, one study examined the relationship between NO scatter [S(NO)] and excited state T_V(NO) values obtained from NO plasmas ($p = 50$ mTorr; at three powers) with either an Si wafer or a Pt foil substrate in the plasma (Fig. 12). Notably, S(NO) values are largely independent of the substrate type (Si wafer versus Pt foil) and increase with increasing P. Scatter values greater than unity indicate surface production of a molecule; therefore, the data from Fig. 12 suggest that as rf P increases, surface production of NO also increases. For each substrate, there is a substantial increase in T_V(NO) at $P = 200$ W, relative to that at 100 W, with that for Pt (~3550 to ~6000 K) being

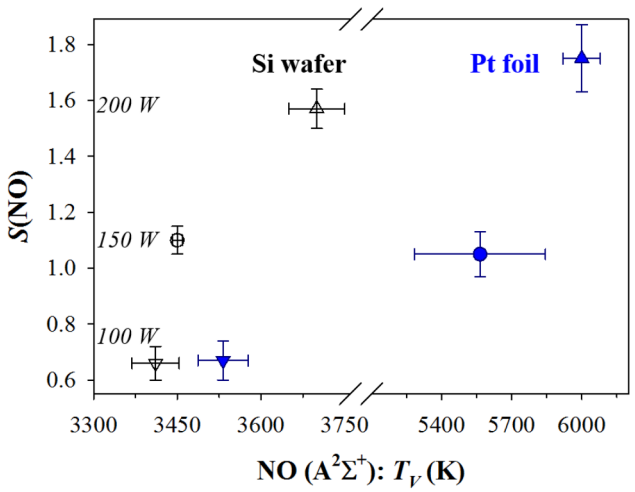

FIG. 12. S(NO) as a function of excited state T_V(NO) values from an NO plasma (p = 50 mTorr) with am Si (open symbols) or Pt foil (closed symbols) substrate present. Bidirectional error bars represent ±1 standard deviation from the mean ($n \geq 3$).

substantially larger than that for Si (~3450 to ~3750 K). For Pt, the 150 W data also show a substantial rise in T_V(NO) (~5550 K) over the 100 W data. One potential hypothesis for this observation is that higher scatter coefficients result from the surface interactions of vibrationally hot molecules. Depicted in Fig. 12, 100 W is the only condition where S(NO) <1, regardless of the substrate, implying surface loss of NO. Notably, this is also the only set of conditions wherein T_V(NO) with a Pt substrate is less than T_V(NO) in the substrate-free system. With an Si substrate in the system, T_V(NO) was lower than T_V(NO) in the substrate-free system under all conditions.[72] As noted above with respect to the SET model,[106,107] this suggests that vibrationally excited molecules interact with the substrate and scatter, having undergone some energy loss, potentially through a resonant energy transfer mechanism. This phenomenon has been previously documented via OES in N_2 plasmas, with both TiO_2 nanoparticles and microstructured zeolites.[82]

To further explore this trend, the plasma reactor (Fig. 2) was lined from end to end with zeolite substrates and a further vibrational cooling was documented. Microplasma generation near and in the pores of these nano- and microstructured materials may be heightened, ultimately leading to enhanced vibrational quenching/resonant transfer interactions with the catalyst surface. Notably, within this study, the presence of a catalyst(s) did not have a clear or significant impact on rotational thermalization pathways.[82] Evaluating steady-state OES provides valuable information regarding energy distributions as well plasma-substrate interactions; however, as noted in Secs. I and II, it is also essential to use temporally resolved spectroscopy to detangle complex plasma dynamics. We also employed TR-OES to study the impact of catalyst(s) on excited state N_2 kinetics,[82] as the coupling of energetic and temporally resolved data is essential to holistically understanding the chemistries within PAC systems.

Although S(NO) does not appear to depend substantially on substrate identity, the presence of the Pt foil resulted in significantly higher T_V values compared to the substrate-free and Si wafer systems, further evidence that the SET mechanism may be contributing to our experimental observations. At all powers studied here, there is substantial scatter of NO off of both substrates, with more than 50% of the molecules desorbing from under all conditions. If we focus on the data from the 200 W systems, however, we observe that S(NO) is significantly greater than unity for both substrates, implying surface production of NO. Surface production of NO could be attributed to several different reactions, a few of which are depicted in reactions (6)–(9),

$$NO^{*}_{(g)} \rightarrow NO_{(ads)} \rightarrow NO_{(g)}, \quad (6)$$

$$NO^{+}_{(g)} \rightarrow NO_{(ads)} \rightarrow NO_{(g)}, \quad (7)$$

$$N_{(g)} + O_{(g)} \rightarrow N_{(ads)} + O_{(ads)} \rightarrow NO_{(ads)} \rightarrow NO_{(g)}, \quad (8)$$

$$N_2O_{(g)} \rightarrow N_2O_{(ads)} \rightarrow NO_{(ads)} + O_{(ads)} \rightarrow NO_{(g)} + O_{(ads)}, \quad (9)$$

where (ads) indicates an adsorbed species, (g) indicates a gas-phase species, and * indicates an excited state species. Note that in reaction (6), we depict an excited state NO molecule desorbing as a ground state molecule, which does not fully describe the internal temperatures of either molecule. Assuming $NO_{(ads)}$ species exist on any given substrate, regardless of how they were formed, they must have sufficient energy to overcome the potential energy barrier for desorption for us to observe them in the IRIS system as surface production of NO. The energy required for desorption of NO from either a Si(111)7 × 7 or a Pt(111) substrate is ~14 kcal/mol (Ref. 109) and ~25 kcal/mol,[110] respectively. The differences in these desorption energy barriers corroborate the notion that vibrationally hot molecules may contribute significantly to higher S values. It also aligns with the observation that a resonant energy transfer mechanism may be at play on the Pt substrate as the SET model allows for a compensation effect whereby vibrational quanta can be added in a stepwise fashion to overcome an activation barrier. Given that it takes more energy for NO radicals to desorb from a Pt surface, we may expect that those molecules may leave the surface vibrationally hotter than ones leaving the Si surface. The data presented here suggest that energy in vibrational modes may preferentially provide a radical with the means to desorb relative to translationally or rotationally hot molecules. Si and Pt substrates were chosen for a noncatalytic and model catalyst system; however, it is important to consider material morphology in addition to chemical identity. Both substrates employed herein are nominally flat and smooth; understanding how radicals scatter from morphologically complex structures may provide more direct evidence of how plasma species synergistically interact with catalytic substrates.[82]

Overall, the combination of the IRIS technique and OES derived data on specific molecules can be employed to study plasma systems with various processing effects on surfaces. Shown here are two systems that have very different processing outcomes from a substrate perspective: NO_x plasmas can oxidize (or nitride) surfaces;[111] CF_4 plasmas are largely used as an etchant, and decreasing the F/C ratio using C_xF_y plasmas leads to film deposition.[112] Thus,

the hypothesis that increasing scatter coefficients result from surface interactions of vibrationally hot molecules was further tested with a variety of FC precursors, shown in Fig. 13.[4] Vibrational temperatures for excited state CF radicals appear to linearly correlate with measured *S*(CF) values. As the vibrational temperature of excited state CF radicals increases, the observed *S*(CF) of the ground state species concomitantly grows. This implies that vibrationally hot CF in excited electronic states contributes significantly to the observed scatter of the ground state species. Excited state CF radicals in the molecular beam may electronically quench at the substrate surface, desorb as ground state CF [i.e., the CF equivalent of reaction (6)], yielding a higher scatter value. Energy from this process may be dissipated into the surrounding FC film or passivation layer being deposited on the surface. The already deposited fluorocarbon film is still receiving the full complement of plasma species and as such can be facilely removed, resulting in a high observed scatter coefficient. Thus, highly vibrationally excited CF may act indirectly as an etchant to ablate FC material.

Consideration of species' vibrational temperature when seeking to optimize any plasma process may increase the ability to tailor and tune experimental conditions. This may be especially relevant for precursors and systems that have competing processes, such as the ability to both etch and deposit, depending on experimental conditions. For example, d'Agostino and co-workers documented that C_4F_{10} and C_2F_6 can etch or deposit, depending on the bias applied to a substrate.[112] By selecting experimental conditions with vibrationally cooler CF, measured by OES, the competition between etching and depositing regimes can be shifted to promote fluorocarbon film formation. The preferential partitioning of energy into vibrational modes correlated with an increased propensity for scatter when a molecule interacts with a substrate, however, does not represent a complete embodiment of the possible surface reactions occurring in these systems. Indeed, as partially depicted in reactions (6)–(9), ion, neutral, and radiation bombardment, vibrational relaxation, decomposition, recombination, and charging of the surface via electron or ion bombardment are all occurring simultaneously.[113] The complexity within these systems exemplifies the need for a comprehensive, holistic approach to plasma diagnostics. Optical spectroscopies can provide insights into how a substrate can modify the plasma discharge itself, ultimately providing means for system optimization, regardless of the end application.

As a final note, although OES is most commonly used to study atomic and diatomic species, it can also be utilized to quantitatively characterize triatomic species (e.g., CF_2), demonstrated in Fig. 14. Figure 14(a) presents an absorbance spectrum of the $\tilde{A}_1B_1$–$\tilde{X}_1B_1$

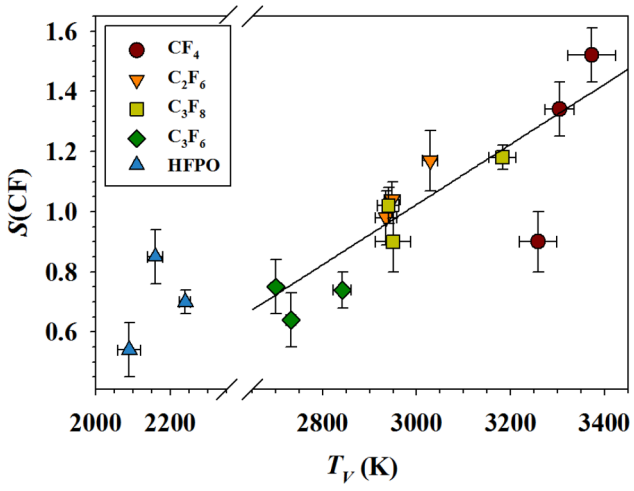

FIG. 13. T_V (K) for CF species in CF_4, C_2F_6, C_3F_8, C_3F_6, and HFPO plasmas as a function of *S*(CF). The linear regression fit to the data for the C_xF_y precursors (i.e., excluding HFPO) yields a slope $m = 0.0010 \pm 0.0002$ with $R^2 > 0.71$. Reproduced with permission from Hanna *et al.*, J. Vac. Sci. Technol. A **35**, 05C308 (2017). Copyright 2017, American Vacuum Society.

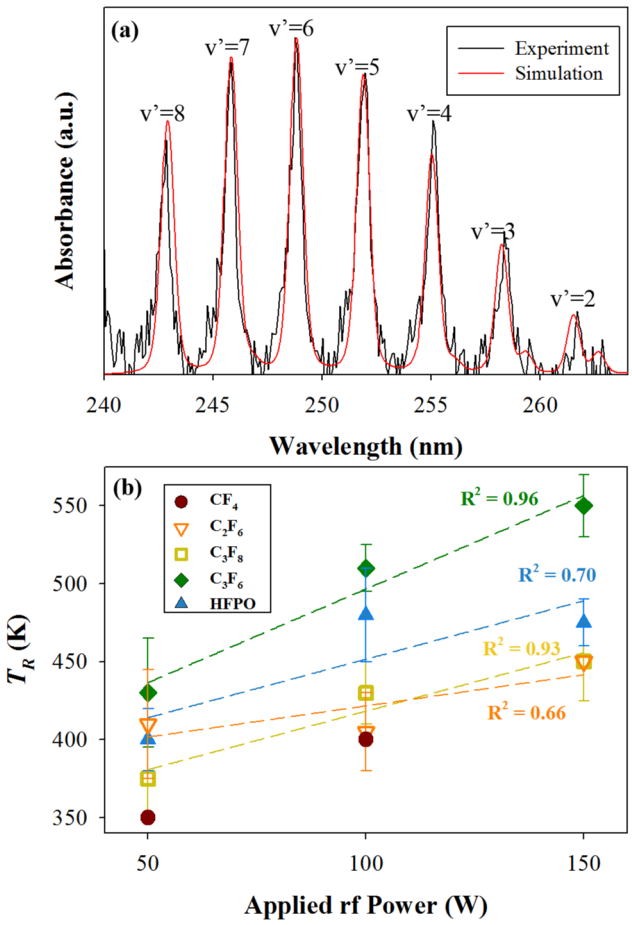

FIG. 14. (a) Absorbance spectrum corresponding to the A^1B_1 (0,v',0) → X^1A_1 (0,0,0) for CF_2 in a C_3F_8 plasma ($p = 50$ mTorr, $P = 50$ W), simulated in PGOPHER, $T_R = 400$ K. (b) T_R for ground state CF_2 species in CF_4, C_2F_6, C_3F_8, C_3F_6, and HFPO plasmas at $p = 50$ mTorr as a function of *P*. R^2 values (all >0.66) corresponding to linear regression fits for each precursor are reported. Reproduced with permission from Hanna *et al.*, J. Vac. Sci. Technol. A **35**, 05C308 (2017). Copyright 2017, American Vacuum Society.

transition for CF_2 in a C_3F_8 plasma ($p = 50$ mTorr, $P = 50$ W) with corresponding fit in PGOPHER, using rotational constants described by Bulcourt *et al.*[114] Here, eight vibrational levels of the ground state were considered in the fit to obtain a single T_R value that is representative of the entire vibrational band.[4] Another approach to determine T_R fits individual vibrational peaks ($v' = 4$, 5, and 6) and then reports an average.[76] Generally speaking, however, the more vibrational transitions included in this method, the more representative the calculated T_R value.

Figure 14(b) details the relationship between $T_R(CF_2)$ and power for a variety of FC precursors. T_R increases linearly with rf P for all precursors, with the data for C_3F_6 and C_3F_8 plasmas exhibiting increased linearity, yielding R^2 values of 0.96 and 0.93, respectively. Described previously, $T_R(CF_2)$ values are approximately 100–200 K higher than $T_R(CF)$.[4] Elevated $T_R(CF_2)$ values suggest that CF_2 molecules produced in these discharges are only partially relaxed by collisions. An increase in P promotes the dissociation of the parent gas and these partially relaxed CF_2 molecules can participate in further fragmentation. This hypothesis could be further investigated by the evaluation of ground state CF radicals; however, CF ($B^2\Delta$–$X^2\Pi$) absorbance peaks arising at ~198 and 202–204 nm (Ref. 115) were undetectable with the current apparatus.[4] Furthermore, the difficulty of determining absorbance of CF_2 at 150 W with high y/x feed gas ratios (i.e., 4 and 3) also suggests that CF_2 ground state molecules are additionally fragmented as more energetic collisions are occurring within the discharge. Cuddy and Fisher reported increased $S(CF_2)$ values compared to $S(CF)$,[62] suggesting that rotationally excited CF_2 are more likely to scatter from a substrate and subsequently participate in further fragmentation processes, potentially forming CF within the discharge. Determination of $T_V(CF_2)$ values within the ground and excited state is necessary to more fully elucidate the mechanisms occurring at the gas-surface interface. Nevertheless, the data presented herein clearly highlight the widespread applicability of nonintrusive optical spectroscopies.

V. SUMMARY AND OBSERVATIONS

Optical spectroscopy provides nonintrusive, *in situ* diagnostic tools (including OES, BAS, and LIF) to examine the complex chemistry in a range of plasma systems. Although OES has been frequently employed for plasma species identification and to elucidate species density with inert gas actinometry, the present work focused on recent literature and new results from the Fisher group that highlight specific ways to significantly enhance and expand these capabilities. The literature is rife with studies that characterized fundamental plasma properties, such as T_e and n_e, within a variety of discharge types and various operating conditions. We have also explored using a simple, OES line ratio technique to explore how these parameters evolve over a range of pressure-power combinations. Using these line ratios, we quantitatively determined power conditions where E to H mode shifts occur at different system pressures. Exploiting the temporal and spectral resolution of our spectrometer allows the collection of TR-OES data, which provides additional insights on the kinetics of species formation within plasma systems. This is especially relevant when applied to the PAC platform that utilizes catalytic substrates.

Perhaps even more powerful, the combination of optical spectroscopies can provide a more comprehensive view of the molecular-level plasma chemistry. Specifically, we used a combination of OES and BAS to document that vibrational energy distributions significantly differ between molecules (N_2 and NO) and electronic states (both excited and ground state) within a given system. Knowledge of internal molecular temperatures and system kinetics for multiple species within a plasma system will significantly aid plasma modeling efforts. Likewise, combining OES with the LIF-based IRIS technique affords insights into the energetics and kinetics, including gas-substrate interactions. It is necessary that a comprehensive understanding of plasma-material interactions include processes that occur at surfaces. Ultimately, many of our results demonstrate that the presence of a substrate in a plasma can dramatically alter the gas-phase chemistry of the system, from both a kinetics perspective and an energetics perspective. Although this might seem obvious, few studies have appropriately documented these effects.

Through optical spectroscopies, the influence of a substrate on the energetics and kinetics of the resulting gas phase has been measured, where efforts to more efficiently tailor plasma processing techniques require a thorough knowledge of both the gas phase and gas-surface interface. Aspects of work detailed here are universally relevant for plasma applications, thus furthering the fundamental understanding of plasma systems required for improved or novel uses. We encourage the plasma community to incorporate optical diagnostic tools more deeply to enhance and enrich their characterization of complex plasma systems.

ACKNOWLEDGMENTS

This work is the culmination of several past and ongoing research projects in the Fisher Group. The authors would like to acknowledge the work of former graduate students who have contributed, especially Joshua M. Blechle and Michael F. Cuddy. The authors also thank Arnold Paecklar for providing assistance and expertise on Python coding as well as the staff of the CSU Central Instrument Facility for valuable conversations about materials characterization. This work was supported by the National Science Foundation (NSF) (No. CBET–1803067) and the American Chemical Petroleum Research Fund (ACS PRF) (No. 59776–ND6).

REFERENCES

[1]J. M. Stillahn, K. J. Trevino, and E. R. Fisher, Annu. Rev. Anal. Chem. **1**, 261 (2008).
[2]A. Grill, *Cold Plasma Materials Fabrications: From Fundamentals to Applications* (IEEE, Piscataway, NJ, 1994).
[3]H. Park and W. Choe, Curr. Appl. Phys. **10**, 1456 (2010).
[4]A. R. Hanna, M. F. Cuddy, and E. R. Fisher, J. Vac. Sci. Technol. A **35**, 05C308 (2017).
[5]O. K. Mawardi, Am. J. Phys. **34**, 112 (1966).
[6]N. Konjević, S. Jovićević, and M. Ivković, Phys. Plasmas **16**, 103501 (2009).
[7]K.-B. Chai and D.-H. Kwon, J. Quant. Spectrosc. Radiat. Transf. **227**, 136 (2019).
[8]A. R. Gizzatullin, Y. O. Zhelonkin, E. F. Voznesencky, and A. R. Gizzatullin, J. Phys. Conf. Ser. **1328**, 012025 (2019).
[9]K. E. Evdokimov, M. E. Konishchev, V. F. Pichugin, A. A. Pustovalova, N. M. Ivanova, and C. Sun, Russ. Phys. J. **60**, 765 (2017).
[10]Z. Navrátil, P. Dvořák, O. Brzobohatý, and D. Trunec, J. Phys. D Appl. Phys. **43**, 505203 (2010).

[11]Y. Yamashita, F. Yamazaki, A. Nezu, and H. Akatsuka, Jpn. J. Appl. Phys. **58**, 016004 (2019).
[12]A. Bogaerts, R. Gijbels, and J. Vlcek, J. Appl. Phys. **84**, 121 (1998).
[13]M. A. Lieberman and A. J. Lichtenberg, *Principle of Plasma Discharges and Materials Processing* (Wiley, New York, 2005).
[14]F. Iza and J. A. Hopwood, IEEE Trans. Plasma Sci. **32**, 498 (2004).
[15]H. W. Drawin, Zeitschrift für Physik **228**, 99 (1969).
[16]J. D. Hey, C. C. Chu, and J. P. S. Rash, J. Quant. Spectrosc. Radiat. Transf. **62**, 371 (1999).
[17]M. Ivković, S. Jovićević, and N. Konjević, Spectrochim. Acta Part B **59**, 591 (2004).
[18]H. Sugai, I. Ghanashev, M. Hosokawa, K. Mizuno, K. Nakamura, H. Toyoda, and K. Yamauchi, Plasma Sources Sci. Technol. **10**, 378 (2001).
[19]F. Taccogna and G. Dilecce, Eur. Phys. J. D **70**, 251 (2016).
[20]J. B. Boffard, R. O. Jung, C. C. Lin, and A. E. Wendt, Plasma Sources Sci. Technol. **19**, 065001 (2010).
[21]J. V. Scanlan and M. B. Hopkins, J. Vac. Sci. Technol. A **10**, 1207 (1992).
[22]B. J. Franek, H. S. Nogami, E. M. Koepke, I. V. Demidov, and V. E. Barnat, Plasma **2**, 65 (2019).
[23]J. B. Boffard, R. O. Jung, C. C. Lin, L. E. Aneskavich, and A. E. Wendt, J. Phys. D Appl. Phys. **45**, 045201 (2012).
[24]S. Siepa, S. Danko, T. V. Tsankov, T. Mussenbrock, and U. Czarnetzki, J. Phys. D Appl. Phys. **47**, 445201 (2014).
[25]X.-M. Zhu and Y.-K. Pu, J. Phys. D Appl. Phys. **43**, 403001 (2010).
[26]A. D. Melnikov, R. A. Usmanov, A. V. Gavrikov, G. D. Liziakin, V. P. Smirnov, R. A. Timirkhanov, and N. A. Vorona, J. Phys. Conf. Ser. **1147**, 012131 (2019).
[27]M. Abrar, A. Qayyum, A. R. Gilani, A. W. Khan, A. Saeed, S. Naseer, and M. Zakaullah, Curr. Appl. Phys. **13**, 969 (2013).
[28]X.-M. Zhu, Y.-K. Pu, Y. Celik, S. Siepa, E. Schüngel, D. Luggenhölscher, and U. Czarnetzki, Plasma Sources Sci. Technol. **21**, 024003 (2012).
[29]A. J. Wu, H. Zhang, X. D. Li, S. Y. Lu, C. M. Du, and J. H. Yan, IEEE Trans. Plasma Sci. **43**, 836 (2015).
[30]S. Wang, A. E. Wendt, J. B. Boffard, C. C. Lin, S. Radovanov, and H. Persing, J. Vac. Sci. Technol. A **31**, 021303 (2013).
[31]S. G. Belostotskiy, T. Ouk, V. M. Donnelly, D. J. Economou, and N. Sadeghi, J. Appl. Phys. **107**, 053305 (2010).
[32]Y.-K. Lee, S.-Y. Moon, S.-J. Oh, and C.-W. Chung, J. Phys. D Appl. Phys. **44**, 285203 (2011).
[33]K. E. Evdokimov, M. E. Konischev, V. F. Pichugin, and Z. Sun, Resour. Effic. Technol. **3**, 187 (2017).
[34]V. M. Donnelly, M. V. Malyshev, M. Schabel, A. Kornblit, W. Tai, I. P. Herman, and N. C. M. Fuller, Plasma Sources Sci. Technol. **11**, A26 (2002).
[35]J. W. Coburn and M. Chen, J. Appl. Phys. **51**, 3134 (1980).
[36]R. A. Gottscho and V. M. Donnelly, J. Appl. Phys. **56**, 245 (1984).
[37]V. M. Donnelly, J. Phys. D Appl. Phys. **37**, R217 (2004).
[38]V. M. Donnelly and A. Kornblit, J. Vac. Sci. Technol. A **31**, 050825 (2013).
[39]N. C. M. Fuller, I. P. Herman, and V. M. Donnelly, J. Appl. Phys. **90**, 3182 (2001).
[40]J. Guha, V. M. Donnelly, and Y.-K. Pu, J. Appl. Phys. **103**, 013306 (2008).
[41]K. A. Alshaltami and S. Daniels, AIP Adv. **9**, 035047 (2019).
[42]M. Kang, Y. Ko, I.-Y. Jang, J. Jung, and J. W. Hahn, Opt. Lett. **42**, 1420 (2017).
[43]M. F. Cuddy and E. R. Fisher, J. Appl. Phys. **108**, 033303 (2010).
[44]E. P. Stuckert, C. J. Miller, and E. R. Fisher, J. Vac. Sci. Technol. B **35**, 021802 (2017).
[45]S. Hirao, Y. Hayashi, and T. Makabe, IEEE Trans. Plasma Sci. **36**, 1410 (2008).
[46]M. Gherardi, N. Puač, D. Marić, A. Stancampiano, G. Malović, V. Colombo, and Z. L. Petrović, Plasma Sources Sci. Technol. **24**, 064004 (2015).
[47]S. Goekce, P. Peschke, C. Hollenstein, P. Leyland, and P. Ott, Plasma Sources Sci. Technol. **25**, 045002 (2016).
[48]R. M. van der Horst, T. Verreycken, E. M. van Veldhuizen, and P. J. Bruggeman, J. Phys. D Appl. Phys. **45**, 345201 (2012).
[49]D. Maletić, N. Puač, N. Selaković, S. Lazović, G. Malović, A. Đorđević, and Z. L. Petrović, Plasma Sources Sci. Technol. **24**, 025006 (2015).
[50]R. R. Jagannath, A. Satija, R. P. Lucht, and S. P. M. Bane, Plasma Sources Sci. Technol. **28**, 01LT02 (2019).
[51]S. Hofmann, K. van Gils, S. van der Linden, S. Iseni, and P. Bruggeman, Eur. Phys. J. D **68**, 56 (2014).
[52]P. Subramonium and M. J. Kushner, J. Appl. Phys. **96**, 82 (2004).
[53]N. Kang, N. Britun, S.-G. Oh, F. Gaboriau, and A. Ricard, J. Phys. D Appl. Phys. **42**, 112001 (2009).
[54]A. Bogaerts, J. Anal. At. Spectrom. **22**, 502 (2007).
[55]X. Yan, Y. Lin, R. Huang, W. Hang, and W. W. Harrison, J. Anal. At. Spectrom. **25**, 534 (2010).
[56]G. P. Jackson and F. L. King, Spectrochim. Acta Part B **58**, 1417 (2003).
[57]J. Lopez, W. Zhu, A. Freilich, A. Belkind, and K. Becker, J. Phys. D Appl. Phys. **38**, 1769 (2005).
[58]A. Belkind, W. Zhu, J. Lopez, and K. Becker, Plasma Sources Sci. Technol. **15**, S17 (2006).
[59]K. Hioki, N. Itazu, Z. L. Petrovic, and T. Makabe, Jpn. J. Appl. Phys. **40**, L1183 (2001).
[60]A. Salmon, N. A. Popov, G. D. Stancu, and C. O. Laux, J. Phys. D Appl. Phys. **51**, 314001 (2018).
[61]M. Bišćan, Z. Kregar, N. Krstulović, and S. Milošević, Plasma Chem. Plasma Process. **30**, 401 (2010).
[62]M. F. Cuddy and E. R. Fisher, ACS Appl. Mater. Interfaces **4**, 1733 (2012).
[63]P. J. Bruggeman, N. Sadeghi, D. C. Schram, and V. Linss, Plasma Sources Sci. Technol. **23**, 023001 (2014).
[64]C.-J. Chen and S.-Z. Li, Plasma Sources Sci. Technol. **24**, 035017 (2015).
[65]Q. Y. Zhang, D. Q. Shi, W. Xu, C. Y. Miao, C. Y. Ma, C. S. Ren, C. Zhang, and Z. Yi, AIP Adv. **5**, 057158 (2015).
[66]F. Yang, Z. Mu, and J. Zhang, Plasma Sci. Technol. **18**, 79 (2016).
[67]S. P. Gangoli, A. F. Gutsol, and A. A. Fridman, Plasma Sources Sci. Technol. **19**, 065003 (2010).
[68]J. Raud, M. Laan, and I. Jogi, J. Phys. D Appl. Phys. **44**, 345201 (2011).
[69]A. Greig, C. Charles, and R. W. Boswell, Phys. Plasmas **23**, 013508 (2016).
[70]R. Ramos, G. Cunge, M. Touzeau, and N. Sadeghi, J. Phys. D Appl. Phys. **41**, 115205 (2008).
[71]I. P. Vinogradov, A. Dinkelmann, and A. Lunk, J. Phys. D Appl. Phys. **37**, 3000 (2004).
[72]J. M. Blechle, A. R. Hanna, and E. R. Fisher, Plasma Process. Polym. **14**, 1700041 (2017).
[73]A. R. Hanna, J. M. Blechle, and E. R. Fisher, J. Phys. Chem. A **121**, 7627 (2017).
[74]P. Bruggeman, G. Cunge, and N. Sadeghi, Plasma Sources Sci. Technol. **21**, 035019 (2012).
[75]A. Wijaikhum *et al.*, Plasma Sources Sci. Technol. **26**, 115004 (2017).
[76]W.-Y. Liu, Y. Xu, Y.-X. Liu, F. Peng, F.-P. Gong, X.-S. Li, A.-M. Zhu, and Y.-N. Wang, Phys. Plasmas **21**, 103501 (2014).
[77]S. Reuter, J. S. Sousa, G. D. Stancu, and J.-P. Hubertus van Helden, Plasma Sources Sci. Technol. **24**, 054001 (2015).
[78]C.-J. Chen, S.-Z. Li, J. Zhang, and D. Liu, J. Phys. D Appl. Phys. **51**, 025201 (2017).
[79]C. M. Western, J. Quant. Spectrosc. Radiat. Transfer **186**, 221 (2017).
[80]J. Luque and D. R. Crosley, SRI International Report MP 99-009, 1999.
[81]C. O. Laux, Presented at the von Karman Institute Lecture Series (2002-07), Rhode-Saint-Genèse, Belgium, 2002 (unpublished).
[82]A. R. Hanna, T. L. Van Surksum, and E. R. Fisher, J. Phys. D Appl. Phys. **52**, 345202 (2019).
[83]T. L. Van Surksum, J. M. Blechle, and E. R. Fisher, J. Vac. Sci. Technol. A **36**, 041302 (2018).
[84]P. R. McCurdy, K. H. A. Bogart, N. F. Dalleska, and E. R. Fisher, Rev. Sci. Instrum. **68**, 1684 (1997).
[85]E. R. Fisher, Plasma Sources Sci. Technol. **11**, A105 (2002).
[86]N. M. Mackie, V. A. Venturo, and E. R. Fisher, J. Phys. Chem. B **101**, 9425 (1997).
[87]P. R. McCurdy, V. A. Venturo, and E. R. Fisher, Chem. Phys. Lett. **274**, 120 (1997).
[88]H.-C. Lee, B. H. Seo, D.-C. Kwon, J. H. Kim, D. J. Seong, S. J. Oh, C. W. Chung, K. H. You, and C. Shin, Appl. Phys. Lett. **110**, 014106 (2017).

[89]H.-C. Lee, D.-H. Kim, and C.-W. Chung, Appl. Phys. Lett. **102**, 234104 (2013).
[90]J. Zhou, I. T. Martin, R. Ayers, E. Adams, D. Liu, and E. R. Fisher, Plasma Sources Sci. Technol. **15**, 714 (2006).
[91]J. T. Gudmundsson, Plasma Sources Sci. Technol. **10**, 76 (2001).
[92]D. L. Crintea, U. Czarnetzki, S. Iordanova, I. Koleva, and D. Luggenhölscher, J. Phys. D Appl. Phys. **42**, 045208 (2009).
[93]A. Durocher-Jean, N. Delnour, and L. Stafford, J. Phys. D Appl. Phys. **52**, 475201 (2019).
[94]J. B. Boffard, S. Wang, C. C. Lin, and A. E. Wendt, Plasma Sources Sci. Technol. **24**, 065005 (2015).
[95]V. A. Godyak, IEEE Trans. Plasma Sci. **34**, 755 (2006).
[96]F. Gao, X.-Y. Lv, Y.-R. Zhang, and Y.-N. Wang, J. Appl. Phys. **126**, 093302 (2019).
[97]E. J. Szili, R. D. Short, D. A. Steele, and J. W. Bradley, in *Surface Modification of Biomaterials*, edited by R. Williams (Woodhead, Cambridge, England, 2011), pp. 3–39.
[98]M. A. Lieberman and S. Ashida, Plasma Sources Sci. Technol. **5**, 145 (1996).
[99]M. D. Logue and M. J. Kushner, J. Appl. Phys. **117**, 043301 (2015).
[100]M. Rybin *et al.*, Carbon **96**, 196 (2016).
[101]D. J. V. Pulsipher, I. T. Martin, and E. R. Fisher, ACS Appl. Mater. Interfaces **2**, 1743 (2010).
[102]A. J. M. Mackus, S. B. S. Heil, E. Langereis, H. C. M. Knoops, M. C. M. van de Sanden, and W. M. M. Kessels, J. Vac. Sci. Technol. A **28**, 77 (2009).
[103]F. R. Gilmore, J. Quant. Spectrosc. Radiat. Transfer **5**, 369–390 (1965).
[104]J. C. Whitehead, J. Phys. D Appl. Phys. **49**, 243001 (2016).
[105]I. Adamovich *et al.*, J. Phys. D Appl. Phys. **50**, 323001 (2017).
[106]R. Larsson, J. Mol. Catal. **55**, 70 (1989).
[107]R. Larsson, Monatshefte für Chemie Chemical Monthly **144**, 21 (2013).
[108]R. Larsson, Molecules **20**, 2529 (2015).
[109]Z. C. Ying and W. Ho, J. Chem. Phys. **91**, 2689 (1989).
[110]N. Kruse, G. Abend, and J. H. Block, J. Chem. Phys. **88**, 1307 (1988).
[111]M. M. Morgan, M. F. Cuddy, and E. R. Fisher, J. Phys. Chem. A **114**, 1722 (2010).
[112]R. d'Agostino, F. Cramarossa, F. Fracassi, and F. Illuzzi, in *Plasma Deposition, Treatment, and Etching of Polymers*, edited by R. d'Agostino (Academic, San Diego, 1990), pp. 95–162.
[113]T. Lafleur, J. Schulze, and Z. Donkó, Plasma Sources Sci. Technol. **28**, 040201 (2019).
[114]N. Bulcourt, J.-P. Booth, E. A. Hudson, J. Luque, D. K. W. Mok, E. P. Lee, F.-T. Chau, and J. M. Dyke, J. Chem. Phys. **120**, 9499 (2004).
[115]J. Luque, E. A. Hudson, and J. P. Booth, J. Chem. Phys. **118**, 622 (2003).
[116]See supplementary material at https://doi.org/10.1116/1.5141844 for a table of the constants used for T_{exc} calculations.

Ellen Fisher is the Assistant Vice President for Strategic Initiatives in the Office of the Vice President for Research at Colorado State University. She is also a Professor of Analytical, Physical, and Materials Chemistry and has served as Department Chair as well as the founding director of a cross-disciplinary initiative, the School of Advanced Materials Discovery (SAMD) from 2014 to 2018. Dr. Fisher received a Bachelor of Science in Chemistry and Mathematics from Texas Lutheran University (formerly College) in 1986 (*summa cum laude*). After attending the University of Utah and receiving her Ph.D. in physical-analytical chemistry in 1991, she performed postdoctoral research at Sandia National Labs before joining the faculty at CSU in 1993. Dr. Fisher has published over 155 peer-reviewed articles spanning diverse topics in plasma science, laser spectroscopy, materials chemistry, chemistry education, and the responsible conduct of research. Dr. Fisher has graduated 19 Ph.D. and 6 M.S. students (1 international); 5 students are currently pursuing the Ph.D. under her guidance, and she has mentored approximately 50 undergraduate research students. For her efforts in research and teaching, she has received the NSF CAREER award and was named an Office of Naval Research Young Investigator as well as a Camille Dreyfus Teacher-Scholar. Dr. Fisher has also received numerous awards from CSU, including the Jack E. Cermak Outstanding Graduate Advisor Award, the Natural Sciences Award for Mentoring Undergraduate Research, the Margaret Hazaleus Award for Empowering Women, and the Oliver P. Pennock Distinguished Service Award. She was recently recognized as a Distinguished Alumnus by the Department of Chemistry at the University of Utah. Prof. Fisher is a Fellow of American Association for the Advancement of Science, the American Chemical Society (ACS), and the American Vacuum Society (AVS). She has served on editorial boards of several technical journals and is currently an Executive Editor of the ACS journal *ACS-Applied Materials and Interfaces*. For her outstanding efforts and excellence in research, teaching, and service, the CSU College of Natural Sciences named her a Professor Laureate in 2009, and in 2010, she was the first woman honored with the University's highest award for research, the Scholarship Impact Award.

One piece of advice Dr. Fisher would give her 16-year old self is to not let the opinions of others (positive or negative) be the overriding guide to your decisions and career path. Too often, we allow ourselves to be influenced by the voices of everyone around us, without stopping to ask some very important questions, including "Is this what **I** really want?"; "How well-aligned are **my** values with those offering opinions to me?"; or even "**Why** am I making the choice that I am making?" Often with age comes perspective—the things that at 16 seem so critical can fade in importance as one becomes older. Realizing that no one path fits all, nor does any single decision decide one's future creates a sense of optimism and hope. It is never too late to change directions, pursue new interests or learn new tricks. The bottom-line advice I would give to my 16-year old self is to always be open to what is possible—regardless of what others may think. That is where the best of science, life, and people always come from.

Angela Hanna is receiving her Ph.D. in Physical Chemistry from Colorado State University under the guidance of Prof. Ellen R. Fisher, expecting to graduate in May 2020. She attended Xavier University in Cincinnati, OH, and completed her B.S. in Chemistry in 2014 with a Minor in Peace Studies (cum laude). Her graduate work focused on understanding fundamental plasma-surface interactions with a holistic approach to plasma diagnostics, ranging from gas-phase spectroscopic investigations to material characterization.